Appendix A Physical derivation of the crushed salt model of Heemann

Table of contents

1 The idealized crystal as a basis of the derivation

Following the argumentation in chapter “compaction by creep of salt” on the linear increase of the width of the contact zone with compaction in case of cubic small salt grains this effect can be captured best by use of the idealized crystal in Fig. A.1. Irrespective of whether the grains are in contact peak to face or edge on edge the width of the contact area must grow linearly with compaction. In the idealized model of peak to peak packed crystals the angle α must be selected such that the free space in the unit cell is equal to the initial porosity of the debris. The angle α is therefore larger for an initially dense packing and thus the peaks of the pyramidal structures will flatten more quickly than in the case of a loose material – in accordance with the above requirement.

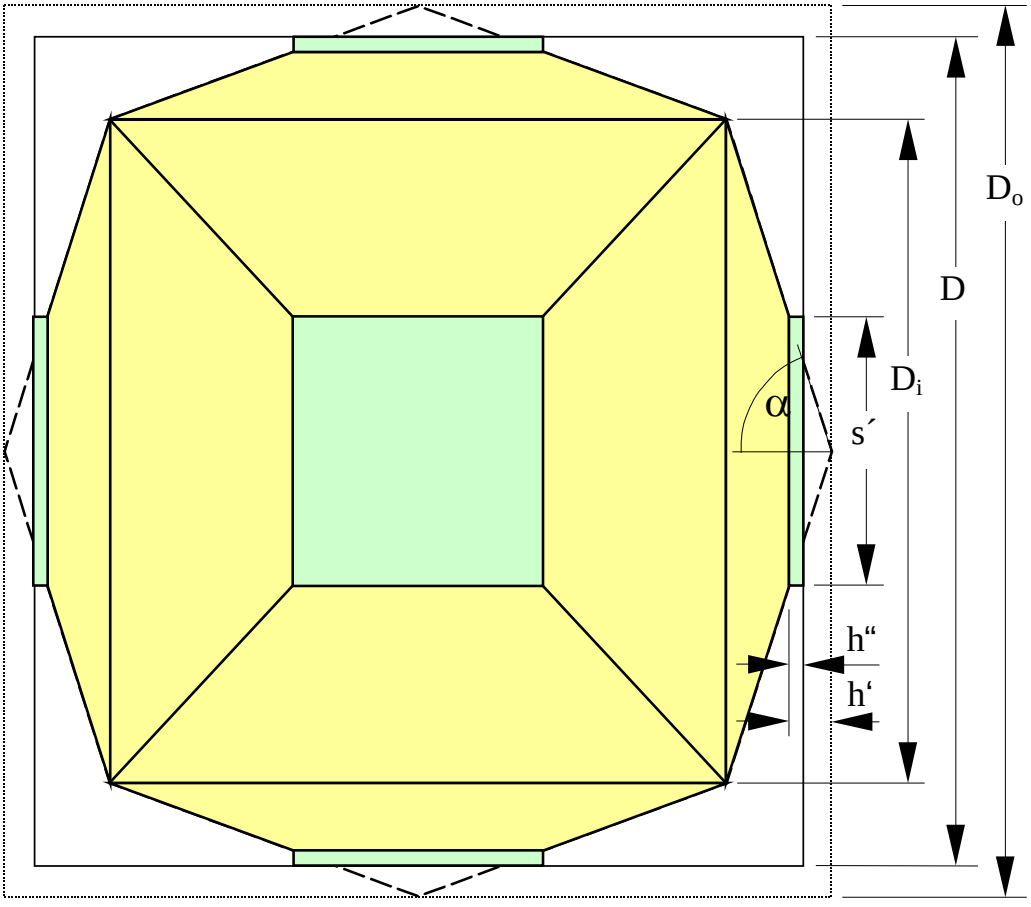

Fig. A.1 Idealized model of a unit crystal with peak to peak contact to six adjoining crystals. Here the crystal can be seen in its initial shape (total width D_0, zero width of contact zone) and after a given deformation (total width D and width s' of contact zone).

This geometric model had first been developed by Stelte (/STE 85/) and very successfully applied for pure compaction. The volume encasing the crystal before compaction is given by

$$V_o = D_o^3 = D_i^3 \left(1+\cot(\alpha)\right)^3. \qquad (A1.1)$$

The index $_o$ declares the initial value. The volume V_s of the salt crystal is given by

$$V_S = D_i^3 \left(1+\cot(\alpha)\right). \qquad (A1.2)$$

The angle α can be taken from the ratio of the two volumes.

$$\frac{V_o}{V_S} = \left(1+\cot(\alpha)\right)^2 = 1+e_o \;\rightarrow\; \cot(\alpha) = \sqrt{1+e_o} - 1. \qquad (A1.3)$$

e_o is the initial void ratio ($e = V_p / V_S$ with the pore volume V_p). In the case of inelastic deformation the relationship between the width s' of the contact zone and its height h' is given by

$$s' = 2h' \tan(\alpha). \qquad (A1.4)$$

Here it is assumed that deformation will be primarily restricted to the contact zone due to the highly non-linear response of creep rate on stress. Because of volume conservation of the salt the height of the deformed zone is given by $h'' = h'/3$. The change in the height of the pyramidal structures is given by $\Delta h = 2/3\, h'$. Thus, for an equal hydrostatic load on all three axes, the unit volume changes by

$$\frac{V}{V_o} = \left(\frac{D}{D_o}\right)^3 = \left(\frac{D_i\left(1+\cot(\alpha)\right) - 2\left(\frac{2}{3}h'\right)}{D_i\left(1+\cot(\alpha)\right)}\right)^3 = \left(1 - \frac{4}{3}\frac{h'}{D_i}\frac{1}{\left(1+\cot(\alpha)\right)}\right)^3 = \frac{1+e}{1+e_o}. \qquad (A1.5)$$

If F is the force on every side of the unit cube the macroscopic pressure p (here assumed to be purely hydrostatic) can be calculated (see eq. (A1.5)) by

$$p = \frac{F}{\left(D_i \left(1+\cot(\alpha)\right) - \frac{4}{3} h' \right)^2} . \qquad \text{(A1.6)}$$

The local uniaxial or deviatoric stress σ within the deformed zone is given by

$$\sigma = \frac{F}{s'^2} = \frac{F}{\left(2 h' \tan(\alpha)\right)^2} = \frac{p}{\left(\frac{2 h' \tan(\alpha)}{D_i \left(1+\cot(\alpha)\right) - \frac{4}{3} h'} \right)^2} = \frac{p}{U}. \qquad \text{(A1.7)}$$

U is the relative contact area and determines the local stress concentration. By inserting eq. (A1.5) into eq. (A1.7), U can be written as a function of the void ratio e:

$$U = \left(\frac{s'}{D}\right)^2 = \left(\frac{2 h' \tan(\alpha)}{D_i \left(1+\cot(\alpha)\right) - \frac{4}{3} h'} \right)^2 = \left(\frac{3}{2} \tan(\alpha) \left(\frac{\frac{4}{3} \frac{h'}{D_i} \frac{1}{1+\cot(\alpha)}}{1 - \frac{4}{3} \frac{h'}{D_i} \frac{1}{1+\cot(\alpha)}} \right) \right)^2 . \qquad \text{(A1.8)}$$

$$= \left(\frac{3}{2} \tan(\alpha) \right)^2 \left(\left(\frac{1+e_o}{1+e} \right)^{1/3} - 1 \right)^2$$

The stationary creep rate can be described to a good approximation by (e.g. /HUN 81/)

$$\dot{\varepsilon} = A \exp\left(\frac{-Q}{RT} \right) \sigma^n . \qquad \text{(A1.9)}$$

σ here is the local deviatoric or uniaxial stress. The creep rate inside the deformed zone and the rate of change of the width of the contact zone are proportional.[1]

[1] The change of height h'' cannot be used because it is also influenced by the mass flowing in from "below".

$$\dot{\varepsilon} = \frac{\frac{d}{dt}\left(s'^2\right)}{s'^2} = 2\frac{\dot{s}'}{s'} = 2\frac{\dot{h}'}{h'} = 2\frac{\dot{h}''}{h''} = A\exp\left(\frac{-Q}{RT}\right)\left(\frac{p}{U}\right)^n \quad \text{where} \quad h'' = \frac{1}{3}h'. \quad (A1.10)$$

The total creep rate is now given by

$$\dot{\varepsilon}_{vol} = \frac{\dot{V}}{V} = 3\frac{\dot{D}}{D} = 3\frac{-\frac{4}{3}\dot{h}'}{D_i\left(1+\cot(\alpha)\right)-\frac{4}{3}h'} = \frac{-2\dot{\varepsilon}h'}{D_i\left(1+\cot(\alpha)\right)-\frac{4}{3}h'} \quad (A1.11)$$

$$= -\dot{\varepsilon}\cot(\alpha)\sqrt{U} = -A\exp\left(\frac{-Q}{RT}\right)\left(\frac{p}{U}\right)^n \cot(\alpha)\sqrt{U}.$$

Up to this point of derivation it had been assumed that deformation only occurs inside the contact zone due to the highly non-linear response of creep rate to stress. But by integrating the creep rate over the total pyramid, creep appears to be about twice that deduced above (eq. (A1.11)). So volumetric creep rate results as

$$\dot{\varepsilon}_{vol} = -2A\exp\left(\frac{-Q}{RT}\right)\left(\frac{p}{U}\right)^n \cot(\alpha)\sqrt{U}. \quad (A1.12)$$

It must be remarked here that the geometric validity of the model is limited to the regime where the width of the contact zone is smaller than the width D_i (see Fig. A.1). That limit is reached when h' comes up to

$$h'_c = \frac{D_i\cot(\alpha)}{2}. \quad (A1.13)$$

By reference to eq. (A1.5) this critical void ratio is given by

$$e_c = \left(\frac{1+\frac{\sqrt{1+e_o}-1}{3}}{\sqrt{1+e_o}}\right)^3\left(1+e_o\right)-1 = \left(\frac{1+\frac{2}{\sqrt{1+e_o}}}{3}\right)^3\left(1+e_o\right)-1. \quad (A1.14)$$

In the regime of $e_o \approx 0.4-0.6$ (roughly equivalent to $n_o \approx 0.3-0.4$) the approximate critical value is given by $e_c \approx 0.01 - 0.02$.

2 Compaction of crushed salt with low porosity

It can be demonstrated both theoretically and by FE analysis that the stationary convergence of drifts and caverns can be described by

$$\dot{\varepsilon}_{vol} = \frac{\dot{V}_{cavern}}{V_{cavern}} = -A\, f\, \exp\left(\frac{-Q}{RT}\right) p^n \qquad (A2.1)$$

where the factor $f \approx 25$ in analytical treatment proves to be only slightly dependent on the geometry of the caverns and their distances. However, the main aspect is the fact that the rate of volume change is proportional to the volume itself. This represents a large discrepancy to eq. (A1.12) for the compaction of crushed salt with medium or high porosity. Looking closer at eq. (A1.12) and eq. (A1.8) it can be seen that the creep rate does not stop at void ratio zero. This is due to the fact that the mathematical description of the pyramids does not take account of their finite height. So eq. (A1.12) must be modified such that for low porosity the description of creep rate in eq. (A1.12) moderately transforms to eq. (A2.1). Eq. (A1.12) can be written as

$$\dot{\varepsilon}_{vol} = \frac{\dot{e}}{1+e} \quad \Rightarrow \quad \dot{e} = -2\, A \exp\left(\frac{-Q}{RT}\right)\left(\frac{p}{U}\right)^n \cot(\alpha)\sqrt{U}\,(1+e). \qquad (A2.2)$$

Eq. (A2.1) can be transformed to a similar form.

$$\frac{\dot{e}}{e} \equiv \frac{\dot{V}_{cavern}}{V_{cavern}} \quad \Rightarrow \quad \dot{e} = -A\, f\, \exp\left(\frac{-Q}{RT}\right) p^n\, e \qquad (A2.3)$$

Both equations can be easily combined by multiplying eq. (A2.2) with the void ratio e.

$$\dot{e} = \dot{\varepsilon}_{vol}\, e(1+e) = -2\, A \exp\left(\frac{-Q}{RT}\right)\left(\frac{p}{U}\right)^{n} \cot(\alpha)\sqrt{U}\, e(1+e) \qquad (A2.4)$$

For large void ratios the creep rate of eq. (A2.4) does not differ to any relevant amount from eq. (A1.12) and geometrically is ruled by the relative contact area U. For a small void ratio U is tending to 1 and the rate of change in the void ratio $\dot{e}$ is proportional to e itself as eq. (A2.3) demands. Transformed back to volumetric strain rates it results as (see eq. (A2.2))

$$\dot{\varepsilon}_{vol} = -2\, A \exp\left(\frac{-Q}{RT}\right)\left(\frac{p}{U}\right)^{n} \cot(\alpha)\sqrt{U}\, e\,. \qquad (A2.5)$$

The factor f, neglected in eq. (A2.4), can be can be taken into account by further parameterisation (see below).

3 Deviatoric creep

If crushed salt is exposed to shear in addition to a hydrostatic load the mathematics of stress tensors show that this general state of stress can always be attributed to pure pressure and tension stresses on the main axes. Vice versa, pressure and tension stresses will appear as shear stresses on some contact zones, depending on their orientation. In the general case of natural grain to grain orientation, locally there will always be pure pressure or pure shear or every possible combination, depending on the orientation of the contact zone. For a given relative contact area U the same stress concentration results and thus the strain rates will be comparable in case of comparable hydrostatic or deviatoric stresses. So the physical/mathematical description of both stress states must be very similar.

In contrast to pure compaction, in the case of deviatoric deformation the inner bulk of the crystal must be taken into account in addition to the pyramidal body, which – in the case of full compaction – takes the full deformation. For a loose material there is only a very low deviatoric creep rate in the bulk. Deviatoric deformation of the pyramids and the bulk

operate in parallel and thus both contributions must be taken into consideration additively. This can be given in its most simple form by

$$\dot{\varepsilon}_{dev} = 2\,A\exp\left(\frac{-Q}{RT}\right)\left(\frac{q}{U}\right)^{n}\cot(\alpha)\sqrt{U}\,c\,e + A\exp\left(\frac{-Q}{RT}\right)q^{n} \qquad (A3.1)$$

with the deviatoric stress

$$q = \sqrt{\frac{3}{2}\sum_{ij}\left(\sigma_{ij}^{macr} - \delta_{ij}\,p\right)^{2}}\,. \qquad (A3.2)$$

The factor c near to 1 is necessary because hydrostatic pressure p cannot be simply replaced by the deviatoric stress q. The same applies to volumetric and deviatoric strain. However, this attempt is still too simplistic, because hydrostatic and deviatoric stresses cannot be considered independently. Theoretical derivation of the complex interactions is excessively difficult. Most phenomenological attempts make use of a potential G to describe a combined hydrostatic and deviatoric load, given by

$$G = \sqrt{h_1(e)\,p^2 + h_2(e)\,q^2}\,, \qquad \dot{\varepsilon}_{ij} = A\exp\left(\frac{-Q}{RT}\right)G^{m}\frac{\partial G}{\partial \sigma_{ij}}\,. \qquad (A3.3)$$

Despite all continuum mechanical reasoning, this attempt is free of physical-geometrical justifications. Because of its multiple use elsewhere it has been tested here by means of finite-element analysis on a unit sphere of salt with a central spherical void, loaded by several combinations of hydrostatic and deviatoric stress. The results fitted the attempt above so well that it has been adopted, including a function $h_2(e)$ (see Appendix Aa) that had been found by fitting. Here, in accordance with that finding, a local stress (in the contact zone) is introduced that fits the physical expectation and the mathematics of the potential above.

$$\sigma_{local} = \sqrt{\left(\frac{p}{U'}\right)^{2} + b\left(\frac{q}{U'^{\beta}}\right)^{2}} \qquad (A3.4)$$

with

$$U' = \left(\kappa\, U\right)^{\gamma}. \qquad \text{(A3.5)}$$

The parameters κ and γ (eq. (A3.5)) here have been introduced to adjust the idealized pyramidal model to better fit real experimental data. A value of $\gamma \approx 0.5$, for instance, would correspond to more rounded edges instead of pyramids. Nevertheless, both values should be very near to 1. The parameters b and β correspond to the function $h_2(e)$ (see eq. (a.2) in Appendix Aa). Eq. (A3.4) must be inserted into eq. (A3.1) replacing the simple deviatoric stress.

$$\dot{\varepsilon}_{dev} = 2\,A \exp\left(\frac{-Q}{RT}\right)\left(\sigma_{local}\right)^{n} \cot(\alpha)\sqrt{U}\, c_e \frac{1}{\sigma_{local}}\left(\frac{q}{U'^{\beta}}\right) + A \exp\left(\frac{-Q}{RT}\right) q^{n} \qquad \text{(A3.6)}$$

The derivation to the stress components as it is done in eq. (A3.3) here has been replaced by a derivation to the local stresses (q / U'^{β} and, see eq. (A3.7) below, p / U'). For low porosity the effect of the first creep term is reduced due to the factor c_e and the main impact is on the second term with simple Norton creep. The hydrostatic stress contribution vanishes completely for $e = 0$. This not only assures a positive void ratio, but also shows that the zone of influence of the effective stress is restricted to a defined sphere around the pore and must thus disappear with it.

The deviatoric and volumetric creep rates must be described in a very similar way. Thus eq. (A2.4) must be replaced by

$$\dot{\varepsilon}_{vol} = -2\,A \exp\left(\frac{-Q}{RT}\right)\left(\sigma_{local}\right)^{n} \cot(\alpha)\sqrt{U}\, \frac{1}{\sigma_{local}}\left(\frac{p}{U'}\right) e. \qquad \text{(A3.7)}$$

4 Grain size distribution

The influence of grain size distribution is assumed to be small in the case of dry crushed salt. However, according to the first characterisation of crushed salt, only the small particles are deformed significantly. In a rather simple approach the crushed salt is divided

up into deforming and non-deforming constituents, attributed to the small and the big grains. Thus the pore volume must be related to the smaller particles which have to close them by strong deformation. When the fraction of the deforming mass to the total mass is given by

$$\frac{m_{comp}}{m_{tot}} = \frac{1}{k}, \qquad (A4.1)$$

the ratio of compacting volume to total volume is given by

$$\frac{V_{comp}}{V_{tot}} = \frac{V_s(1+k\,e)}{V_s(k-1)+V_s(1+k\,e)} = \frac{1+k\,e}{k(1+e)} = \frac{k^{-1}+e}{1+e}. \qquad (A4.2)$$

The global compaction rate is reduced by a factor of V_{comp}/V_{tot} (see eq. (A4.2)) compared to the compaction rate of the unit crystal in Fig. A.1.

$$\dot{\varepsilon}_{vol}(k) = \dot{\varepsilon}_{vol}\frac{k^{-1}+e}{1+e} \qquad (A4.3)$$

The porosity of the total pile must now be concentrated in the smaller deforming fraction represented by the idealized grain model. A "local void ratio"

$$e_{local} = k\,e \qquad (A4.4)$$

must be adopted for the compacting fraction and the geometric function U must be replaced by

$$U = U(e_{local}) = \left(\frac{3}{2}\tan(\alpha)\right)^2\left(\left(\frac{1+k\,e_o}{1+k\,e}\right)^{1/3}-1\right)^2 \qquad (A4.5)$$

where

$$\cot(\alpha) = \sqrt{1+k\,e_o}-1. \qquad (A4.6)$$

5 Hardening

Rock salt displays the phenomenon of hardening leading to a reduction in creep rate (or increase in stress). If sufficient time is allowed, the mechanism tends towards a stationary state with constant stress and strain rate. In theory this is described very elegantly by means of an inner hardening stress σ_R which can be attributed physically to the interaction of the deformation-bearing dislocations. The experimental results in Appendix Ab show that this phenomenon is also found in crushed salt. This hardening mechanism is described in Appendix Ac and the differential equation defining the evolution of this hardening stress is derived. The creep rate can then be given by a differential equation of this type

$$\dot{\varepsilon}^{creep} = \dot{\varepsilon}^{creep}\left(\sigma_{eff}\right) = \dot{\varepsilon}^{creep}\left(\sigma - \sigma_R\right) \qquad \text{(A5.1)}$$

including a differential equation for the evolution of the hardening stress σ_R.

$$\frac{d\sigma_R}{d\varepsilon^{creep}} = \kappa_R \left(\frac{\sigma_{eff}}{\sigma_R} - \left(\frac{1-z}{z} \right)^2 \frac{\sigma_R}{\sigma_{eff}} \right) \qquad \text{(A5.2)}$$

This physical description of hardening applies inside the core (bulk) of the grain but is not applicable in the pyramidal parts of the geometrical model due to the highly heterogeneous stresses there. A phenomenological model for the hardening stress σ_{RV} in the contact zone must be used because it is always extended by low hardened material from beneath, disallowing analytical treatment. However, the relationship found in Appendix Ac qualitatively meets the anticipated evolution and tends to the right limit.

$$d\sigma_{RV} = \frac{\sigma_{RV} - z\,\sigma_{local}}{m\,\varepsilon_v} d\varepsilon_v \qquad \text{(A5.3)}$$

The smaller the parameter m is the faster and closer the hardening stress will approach the anticipated limit $z\,\sigma_{local}$. m is thus an appropriate phenomenological parameter in the order of $m \approx 0.2 - 0.5$.

6 Unified description

Taking account of all theoretical, numerical and phenomenological consideration, the optimal combination of the upper equations is given by

$$\dot{\varepsilon}_{vol} = -2\,A\exp\left(\frac{-Q}{RT}\right)\left(\frac{\sigma_{local}-\sigma_{RV}}{1-z}\right)^{n-1}\cot(\alpha)\sqrt{U}\left(\frac{p}{U'}\right)e\frac{k^{-1}+e}{1+e}, \qquad (A6.1)$$

$$\dot{\varepsilon}_{dev} = 2\,A\exp\left(\frac{-Q}{RT}\right)\left(\frac{\sigma_{local}-\sigma_{RV}}{1-z}\right)^{n-1}\cot(\alpha)\sqrt{U}\,c\left(\frac{q}{U'^{\beta}}\right)e\frac{k^{-1}+e}{1+e} + A\exp\left(\frac{-Q}{RT}\right)\left(\frac{q-\sigma_R}{1-z}\right)^{n} \qquad (A6.2)$$

with

$$\sigma_{local} = \sqrt{\left(\frac{p}{U'}\right)^2 + b\left(\frac{q}{U'^{\beta}}\right)^2}, \qquad (A6.3)$$

$$U = \left(\frac{3}{2}\tan(\alpha)\right)^2\left(\left(\frac{1+k\,e_o}{1+k\,e}\right)^{1/3}-1\right)^2, \qquad (A6.4)$$

$$\cot(\alpha) = \sqrt{1+k\,e_o}-1, \qquad (A6.5)$$

$$U' = (\kappa\,U)^{\gamma}. \qquad (A6.6)$$

The evolution of resistive stress is given by the equations (A5.2) and (A5.3). The hardening stress σ_{RV} is active in the pyramidal creep terms only. Its influence has been scaled by dividing the effective stresses $(\sigma_{local}-\sigma_{RV})$ and $(q-\sigma_R)$ by $(1-z)$ so that in the case of stationary creep the same creep rate is always reached irrespective of the value of z.

The parameters for the creep equations were identified in the context of the BAMBUS project, making use of 85 experimental volumetric and deviatoric creep rates (see /KOR 96/) for different temperatures, stresses and void ratios, without taking hardening into account. The logarithmic standard deviation between model and experimental data was determined for different sets of parameters (see Tab. A.1).

These parameters were found by adopting the usual parameters (see /HUN 81/) for rock salt creep as fixed values.

$A = 0.18\ d^{-1}\ MPa^{-5}$
$Q = 54$ kJ/Mol
$n = 5$

and the gas constant

$R = 8.3143$ J/(K Mol).

Tab. A.1 Parameter sets for eq. (A6.1) to (A6.6) for different grades of optimization and the resulting standard deviation.

	Not optimised	Partially optimised (k=1)	Partially optimised (k=3)	Manually adjusted (k=6)	Fully optimised
κ	1	0.971	1.151	1.41	2.641
γ	1	0.997	0.896	0.84	0.720
b	1	3.617	3.075	2.53	1.373
β	1	0.705	0.755	0.82	0.956
c	1	0.853	0.855	0.85	0.841
k	1	1	3	6	24.631
Std. dev.	0.716	0.656	0.608		0.554

Even without any parameter optimization, the logarithmic standard deviation shows a very low value corresponding to a mean factor of 2.05 between the model and Korthaus' experimental data. The second parameter set corresponds to a model with uniform grain size ($k=1$) where all grains contribute to compaction. The parameter k cannot be determined easily and has been conservatively estimated as $k=3$ in the third set. In both cases the parameters did not deviate greatly from 1 except for the parameters b and β, which are very similar to the parameters found in the numeric simulation (compare eq. (

a.2) in Appendix Aa). For full optimization the value of $k \approx 24.6$, in particular, appears to be far beyond the reasonable range. So, despite the better numerical agreement of experimental data and model, it is physically not very reliable. The set with the conservative value $\mathrm{k}=3$ therefore got the highest degree of trust at that point of development.

A later estimation of k on the basis of the given grain size distribution used by Korthaus makes a value of $5 < k < 7$ appear reasonable (see Appendix Ae). So, manually a parameter set for $\mathrm{k}=6$ was adjusted (no standard deviation determined). A graphical representation of the creep curves in Fig. A.2 ($\dot{\varepsilon}$ for pure hydrostatic load with $p = 1 MPa$ for $T = 300\,K$) for all five parameter sets shows their agreements and deviations.

The five curves in Fig. A.2 represent the non-optimized model (ePkt(BGR), black line, see also Tab. A.1) as well as the models for $\mathrm{k}=1$, $\mathrm{k}=3$ and $\mathrm{k}=6$ and the fully optimized model in red (ePkt(BGR, k=24.63)) best representing the experimental data.

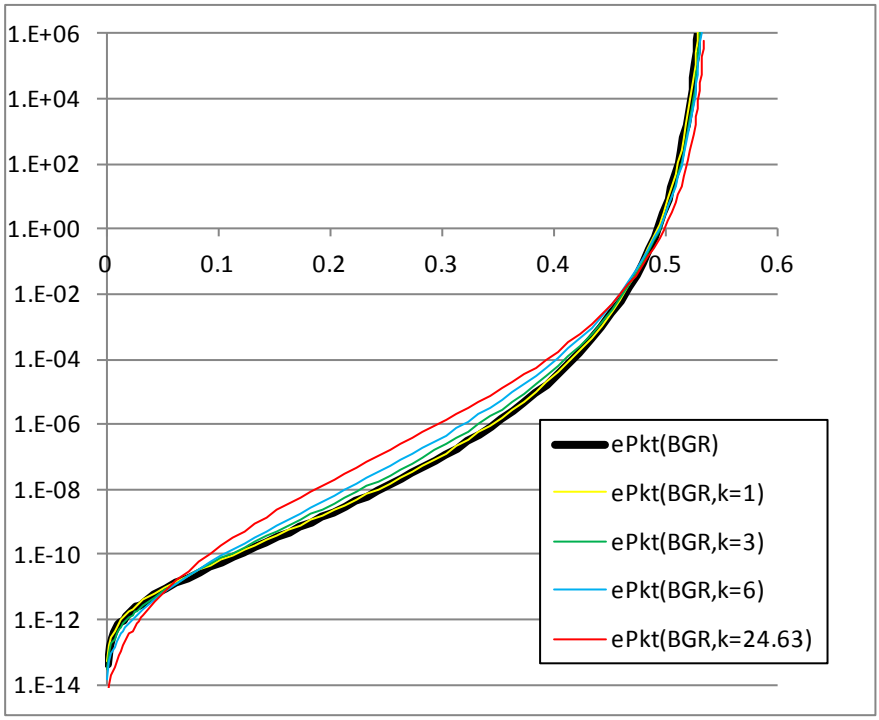

Fig. A.2 Creep rate over void ratio for five parameter sets. The black curve represents the non-optimized model, the red curve the fully optimized one.

7 Creep with allowance for hardening

The parameterized creep curves in Fig. A.2 have been calculated for quasi-stationary creep and fitted without taking regard of hardening. Principally, fitting the hardening parameters only requires determination of the parameters m, κ_R and z. The parameter κ_R will be effective only for a high grade of compaction so that attempting to fit it to experimental data with void ratios bigger than $e > 0.05$ will not be very successful. The parameter z is known to lie between $0.6 \le z \le 0.7$. Both parameters might also be better determined by comparison with rock salt data. Reasonable accuracy can be achieved by adopting a value of $z = 0.65$ and $\kappa_R \approx 225\,MPa$. This means that only the value of m must be determined by inverse modelling. A preliminary value is given by $m \approx 0.3$.

8 On the elastic stiffness of crushed salt

Analytical determination of the elastic stiffness is based on the assumption that the stored energy of a body (resulting from a global stress σ_{global}) is directly related to its stiffness.

$$W_{tot} = \frac{\sigma_{global}^2}{2C'} V_{tot} = \int_{V_{tot}} \frac{\sigma_{local}^2}{2C''} dV \qquad \text{(A8.1)}$$

C' is the stiffness characterizing the global stiffness as it has to be used in numerical calculations while C'' is the local stiffness. While the stresses inside larger grains or the cores of the fine grains are comparable to the global stresses, the local stresses in the contact zones are much higher and thus the total stored energy there. The material stiffness can be supposed to be the same at every point of the salt ($C'' = C$). Thus, in the case of higher stored energy, an effectively lower stiffness $C' < C$ results compared to that of compact salt. This general relationship is independent of whether deviatoric or hydrostatic stresses are used. As a consequence of the same, geometrically given stress intensification factors for both deviatoric or hydrostatic stresses, their relative development with change of geometry is identical and thus also the development of the shear modulus and the bulk modulus. Poisson's ratio is therefore unchanged during

compaction. This conclusion is correct as long as the stresses resulting from lateral contraction can be neglected. It is assumed that this is the case.

The attempt to calculate the stored energy of a crushed salt grain (see Appendix Ag) cannot return precise results due to the assumption above and the necessarily simple assumptions made about the geometry of the grains. Nevertheless, the geometric model in Fig. A.1 provides a good basis for calculating the relative stiffness. Unfortunately the question on the influence of the non-compacting constituent of coarse grains still could not be answered satisfactorily. Thus the character of the curves for stiffness as a function of void ratio must be regarded as being unclarified (see Appendix Ag). However, it is plausible to anticipate an almost linear course with void ratio.

$$C_{crushed\ salt} = C_{salt}\left(1 - \frac{e}{e_o}\right) \qquad \text{(A8.2)}$$

Though the true development of C as a function of grain size distribution (governed by k) may deviate slightly from eq. (A8.2), its influence on numerical modelling will be sufficiently small to allow it to be used.

9 Humidity creep

The basic idea of the mechanism of humidity creep is based on the expectation that a very thin layer of mainly crystalline water exists in the contact area between two grains, where – due to the strong ionic forces of water and salt – salt ions can easily be dissolved and move diffusively. Under the action of a driving potential on the contact area a salt ion will primarily migrate in the direction of the lower potential.

The chemical potential H of a crystalline bound ion is proportional to the normal pressure σ_n.

$$H = -\kappa\,\sigma_n \qquad \text{(A9.1)}$$

If an ion is leaving its bound state it needs a certain amount Q of energy – taken from thermal movement. Q is referred to as the activation energy for this process. The probability of such a process is known from stochastic physics to be given by

$$P = A\exp\left(-\frac{Q}{k_B T}\right). \qquad \text{(A9.2)}$$

The parameter k_B is known as the Boltzmann constant, T represents temperature. When the particle in its temporarily mobile state is able to change its position slightly (may be a lattice constant b) in two directions (forwards, backwards), there are two different probabilities due to the further energy from the chemical potential that increases or reduces the effective activation energy.

$$P^{+} = A\exp\left(-\frac{Q+\Delta H^{+}}{k_B T}\right) = A\exp\left(-\frac{Q-\kappa\, grad\left(\sigma_n\right)b}{k_B T}\right) \qquad \text{(A9.3)}$$

$$P^{-} = A\exp\left(-\frac{Q+\Delta H^{-}}{k_B T}\right) = A\exp\left(-\frac{Q+\kappa\, grad\left(\sigma_n\right)b}{k_B T}\right) \qquad \text{(A9.4)}$$

Here, the gradient of the potential H and thus the gradient of the pressure σ_n is taken to be negative in positive r-direction. The particles moving in positive and negative directions balance their opposing action if they are of equal amount. The number of particles that effectively migrate in the positive direction can be calculated from the difference of their probabilities.

$$\begin{aligned}
&\Delta r^{eff} = P^{eff}\, b = \left(P^{+} - P^{-}\right)b \\
&= \left(A\exp\left(-\frac{Q-\kappa\, grad\left(\sigma_n\right)b}{k_B T}\right) - A\exp\left(-\frac{Q+\kappa\, grad\left(\sigma_n\right)b}{k_B T}\right)\right)b \\
&= A\exp\left(-\frac{Q}{k_B T}\right)\left(\exp\left(\kappa\frac{grad\left(\sigma_n\right)b}{k_B T}\right) - \exp\left(-\kappa\frac{grad\left(\sigma_n\right)b}{k_B T}\right)\right)b \\
&= 2\,A\exp\left(-\frac{Q}{k_B T}\right)\sinh\left(\kappa\, b\frac{grad\left(\sigma_n\right)}{k_B T}\right)b.
\end{aligned} \qquad \text{(A9.5)}$$

The mean velocity v a particle will have in the direction of the driving potential by means of the thermal lattice frequency ν_0 is then given by

$$\begin{aligned} \mathrm{v} &= \nu_o \, \Delta r^{eff} = \nu_0 \, b \, 2 \, A \exp\left(-\frac{Q}{k_B T} \right) \sinh\left(\kappa b \frac{grad\left(\sigma_n\right)}{k_B T} \right) \\ &= D' \exp\left(-\frac{Q^{diff}}{R^{gas} T} \right) \sinh\left(\kappa' \frac{grad\left(\sigma_n\right)}{T} \right) \end{aligned} \qquad \text{(A9.6)}$$

with

$$D' = 2 \nu_0 \, b \, A \,, \qquad \text{(A9.7)}$$

$$\kappa' = \frac{\kappa b}{k_B} . \qquad \text{(A9.8)}$$

In eq. (A9.6) the Boltzmann constant k_B has been replaced by the general gas constant R^{gas}. The necessary change in the definition of Q is done by introducing the new activation energy Q^{diff}, which is taken as the activation energy for this diffusive process.

Consider a contact area of radius R (see Fig. A.3) with a radially varying normal pressure defining the potential (see Fig. A.4). To uniformly extract a layer of material out of this area by diffusion (with a resulting sink rate $\dot{h}$) a radial flux of matter proportional to the inner area must exist.

$$\dot{m} = \rho \, b \, 2 \pi \, r \, \mathrm{v} = \rho \, \pi \, r^2 \, \dot{h} \qquad \text{(A9.9)}$$

In eq. (A9.9) the height of the transport layer has been set (somewhat arbitrarily) to the lattice constant b. The diffusion flux (also see eq. (A9.6)) is then given by

$$\mathrm{v} = \frac{r \, \dot{h}}{2 b} = D' \exp\left(\frac{-Q^{diff}}{R^{gas} T} \right) \sinh\left(\kappa' \frac{grad\left(\sigma_n\right)}{T} \right) . \qquad \text{(A9.10)}$$

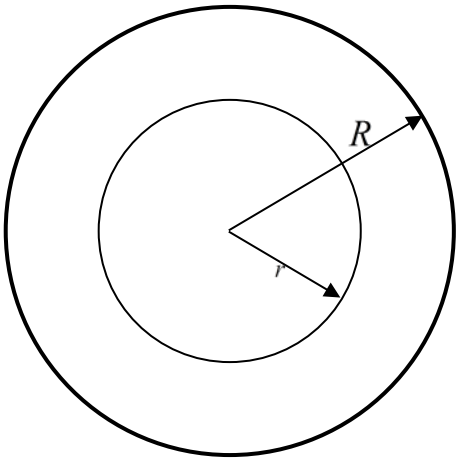

Fig. A.3 Circular contact area of radius R.

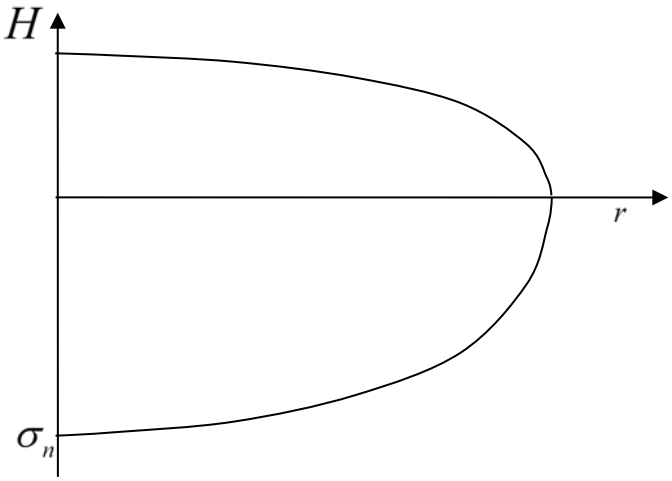

Fig. A.4 Qualitative line of normal stress σ_n and potential H.

So the gradient of the stress σ_n can be extracted.

$$grad\left(\sigma_n\right)=\frac{\partial\sigma_n}{\partial r}=\frac{T}{\kappa'}\operatorname{arsinh}\left(\exp\left(\frac{Q^{diff}}{R^{gas}\,T}\right)\frac{r\,\dot{h}}{2\,b\,D'}\right) \qquad \text{(A9.11)}$$

The rate for the height h can be found by integration of this differential equation (see Appendix Ah) and resolving it to $\dot{h}$.

$$\dot{h}\cong -2.7\,\frac{b}{R}\,D'\exp\left(\frac{-Q^{diff}}{R^{gas}\,T}\right)\sinh\left(\frac{\bar{\sigma}_n\,3\kappa'}{T\,R}\right) \qquad \text{(A9.12)}$$

In case of pure humidity creep the rate of height $\dot{h}$ can easily be connected to the rate of volume. The compaction rate (compare eq. (A1.5)) is given by

$$\begin{aligned}\dot{\varepsilon}_{vol}^{diff} &= \frac{\dot{V}}{V} = 3\frac{\dot{D}}{D} = 3\frac{2\dot{h}}{D_o\left(\frac{1+k\,e}{1+k\,e_o}\right)^{1/3}} = 6\left(\frac{1+k\,e_o}{1+k\,e}\right)^{1/3}\frac{\dot{h}}{D_i\left(1+\cot(\alpha)\right)} \\ &= -16.2\left(\frac{\left(1+\cot(\alpha)\right)^2}{1+k\,e}\right)^{1/3}\frac{b}{R}D'\exp\left(\frac{-Q^{diff}}{R^{gas}\,T}\right)\sinh\left(\frac{\bar{\sigma}_n\,3\kappa'}{T\,R}\right) \\ &= -\frac{16.2\,b\,D'}{R\,D_i\left(\left(1+\cot(\alpha)\right)\left(1+k\,e\right)\right)^{1/3}}\exp\left(\frac{-Q^{diff}}{R^{gas}\,T}\right)\sinh\left(\frac{\bar{\sigma}_n\,3\kappa'}{T\,R}\right).\end{aligned} \qquad \text{(A9.13)}$$

In eq. (A9.13), the increased "local" void ratio around the fine grains (see eq. (A4.4)) has been inserted, but the proportion of compacting fine material and non-compacting coarse material (see eq. (A4.3)) must still be incorporated to calculate the total compaction rate. With the summarised diffusion constant

$$D^{diff} = 16.2\,b\,D' \qquad \text{(A9.14)}$$

the compaction rate is given by

$$\begin{aligned}\dot{\varepsilon}_{vol}^{diff}(k) &= \dot{\varepsilon}_{vol}^{diff}\frac{V_{comp}}{V_{tot}} = \dot{\varepsilon}_{vol}^{diff}\frac{1+k\,e}{k\left(1+e\right)} \\ &= -\frac{D^{diff}}{R\,D_i\left(1+\cot(\alpha)\right)^{1/3}}\frac{\left(1+k\,e\right)^{2/3}}{k\left(1+e\right)}\exp\left(\frac{-Q^{diff}}{R^{gas}\,T}\right)\sinh\left(\frac{\bar{\sigma}_n\,3\kappa'}{T\,R}\right).\end{aligned} \qquad \text{(A9.15)}$$

D_i is the typical length of a unit cell (see Fig. A.1) of a grain in the initial loose state and essentially can be identified with the smallest effective grain size. In a final step the diameter of the contact area must be found. Here it is implied that the salt leaving the contact area accumulates immediately in the neighbourhood of the gap, so that the resulting geometry is the same as in the case of the dry crushed salt (see Fig. A.1). With recourse to eq. (A1.5) and (A1.4) the radius R can be taken as half of the diameter s', except for a factor $\varsigma \geqslant 1$.

$$R = \varsigma \frac{s'}{2} = \varsigma \frac{3}{4} \frac{D_i\left(1+\cot\left(\alpha\right)\right)}{\cot\left(\alpha\right)} \left(1 - \left(\frac{1+k\,e}{1+k\,e_o} \right)^{\frac{1}{3}} \right) \qquad \text{(A9.16)}$$

So humidity creep is – in contrast to dry deformation – inversely proportional to the cube of the grain diameter, in agreement with expectations (for sufficiently small stresses). However, the individual diffusion process on a contact area is inversely proportional to the square of the current radius (for small stresses again).

9.1 Deviatoric humidity creep

In the case of pure shear on a contact area, only weak diffusive transport is theoretically necessary. One can imagine that short diffusion distances must be overcome on a non-planar contact area (see Fig. A.5).

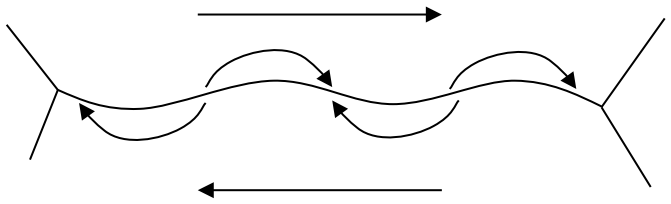

Fig. A.5 Diffusion transport on a wavy contact area to overcome incompatibilities of surface geometry in the case of pure shear.

However the more general case of contact areas at a certain angle to shear direction usually will be the dominant process (see Fig. A.6). Both crystals have to reduce their heights by diffusion (analogous to dry deformation). So a deviatoric (shear) deformation of the pile is possible. It must therefore be assumed that the combined local stress for dry crushed salt also is valid for humid crushed salt. Diffusion creep can therefore be described by

$$\dot{\varepsilon}_{ij}^{diff} = -\frac{D^{diff}}{R\,D_i\left(1+\cot(\alpha)\right)^{1/3}}\frac{\left(1+k\,e\right)^{2/3}}{k\left(1+e\right)}\exp\left(\frac{-Q^{diff}}{R^{gas}\,T}\right)\sinh\left(\frac{\sigma_{local}\,3\kappa'}{T\,R}\right)\frac{\partial\sigma_{local}}{\partial\sigma_{ij}^{local}}$$

$$= -\frac{D^{diff}}{R\,D_i\left(1+\cot(\alpha)\right)^{1/3}}\frac{\left(1+k\,e\right)^{2/3}}{k\left(1+e\right)} \qquad \text{(A9.17)}$$

$$\exp\left(\frac{-Q^{diff}}{R^{gas}\,T}\right)\sinh\left(\frac{\sigma_{local}\,3\kappa'}{T\,R}\right)\frac{1}{\sigma_{local}}\left(\frac{p}{U'}\frac{\delta_{ij}}{3}+c_d\,\frac{q}{U'^{\beta}}\frac{3}{2}\frac{q_{ij}}{q}\right)$$

with the still undetermined parameter $c_d \approx 1$.

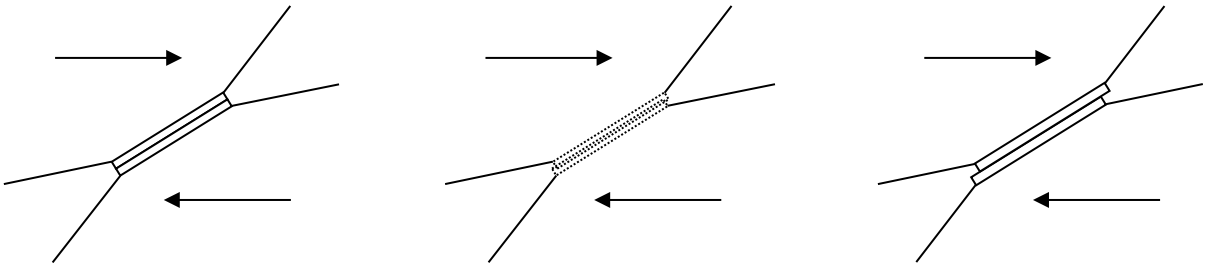

Fig. A.6 For combined pressure and shear a height reduction in the contact zone combined with a broadening and thus still greater height of the contact volume (see part c) will appear in order to avoid interpenetration of the two crystals (see part b).

9.2 Humidity creep for small void ratio

In contrast to dry creep, even in the framework of the geometric model in Fig. A.1, the diffusive processes can continue until the remaining space is completely closed (see Fig. A.7). In fact, a limited contact area curvature will appear, due to the different diffusion lengths for different directions at an early state of deformation. In the case of small residual porosities this will lead to a distinct reduction in permeability (up to total closure despite residual porosity, also see Fig. A.8). In the case of total closure, on the other hand, the free area where diffusion is possible is increasingly reduced.

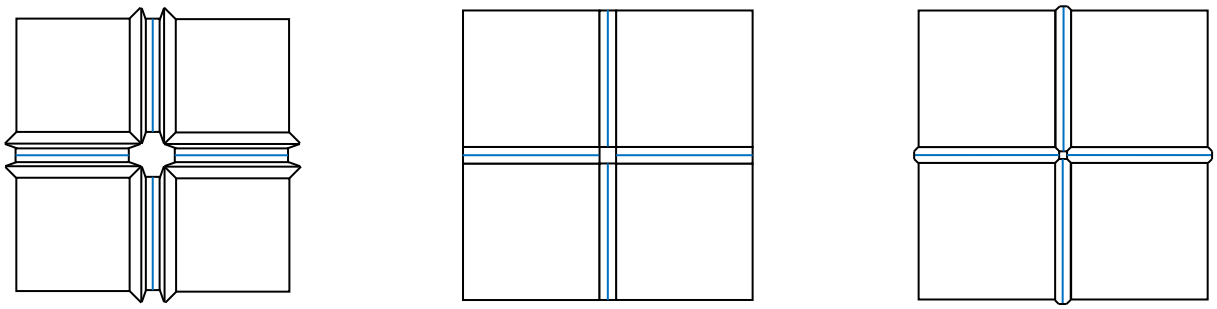

Fig. A.7 Development of void space between four crystals in the case of humidity creep for a very small rest porosity.

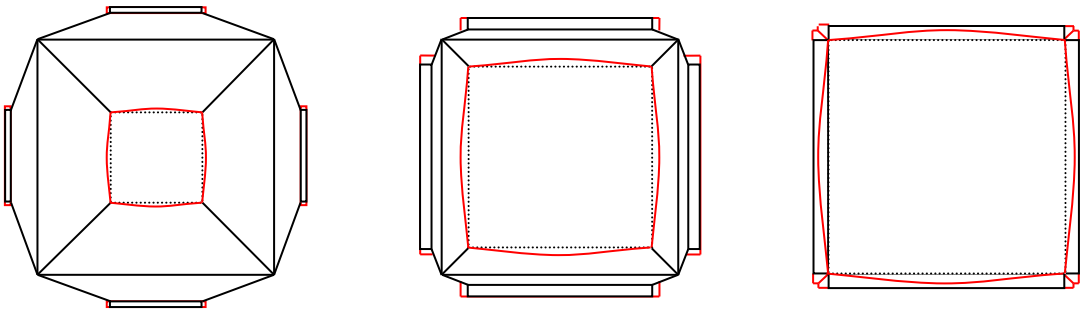

Fig. A.8 The transmissibility of the remaining pore structure will be substantially reduced for small porosities due to a certain curvature of the contact area as a consequence of the diffusive process.

Whether or not this limiting state will require more detailed modelling (irrespective of a realistic result) is a question of future research and development. A reliable model for the development of permeability, which in consequence may prohibit further closure because of relevant amounts of liquid and gas, remains very important to numerical analysis.

10 Evaluation of current status and need for further development

The model in principle is able to describe creep of dry and crushed salt. It is based on a geometrical model that takes account of the cubic shape of the fine grains in crushed salt. It takes account of the grain size distribution my means of a separation into compacting fine grains and big grains that scarcely participate in compaction. A new attempt has been incorporated to model effects of grain fracture that influence the relative positions of the grains and by this way also influence creep of the crushed salt that is determined by the properties of salt and geometry of the grains. It also incorporates a model on hardening of the grains due to deformation.

Principally the model of creep of dry crushed salt gives very good results what has been proven already in case of the benchmark calculations within the BAMBUS-project /BEH 04/. From a practical point of view the behaviour of the model for a rather loose status is not very important due to the development of rather low pressure under in-situ-conditions that will not substantially affect the convergence of the host rock. With raising stress this will change until high compaction is reached. Unfortunately the creep rates that will appear in situ are far below that in laboratory so that the reliability of the physical model is essential. The theoretical research on hardening effects not only could prove that the exponent of stress in the Norton-type creep model is similar to that of salt. It also could combine the results on rock salt /HAM 07/ and those of Korthaus /KOR 96/ and Stührenberg & Zhang /STÜ 95a/, /STÜ 95b/ on crushed salt that seemed to be inconsistent. So this work gives a high degree of reliability in the stress dependency of the model. Nevertheless, the numerical calculations within REPOPERM have been done with a stress exponent of 5 while experimental findings (/HAM 07/) and theory (not circumstantiated here) suggest an exponent 7. In fact, it might be even better to make use of a hyperbolic stress dependency which is supposed to better describe stress and temperature dependency.

The dependency of creep rate on the void ratio has been modelled by means of the geometrical model that has firstly been developed by Stelte /STE 85/. Even without fitting of any parameter it was able to reproduce the experimental results very well (see section 3.3.1 in the main report). So the equations found by geometrical and physical reasoning seem to be very near to physical reality. Nevertheless, for small void ratios the model

involves a process of compaction that deviates from that of low or medium dense material. Though there is a natural link between those two regimes due to the lack of reliable data on small pores this part of description could not be tested so far.

There is some evidence that for very loose material grain fracture will influence also the behaviour of highly compacted crushed salt by means of the related grain rearrangement affecting the geometric positions of neighbouring grains. An approach to simulate that influence has been developed but not been tested yet.

The model involves also the influence of grain size distribution allowing a better fitting to experimental results. That might be rather important in case of grain size separation during in-situ-emplacement where the laboratory results will have to be extrapolated as far as there are not sufficient data on that. Despite any physical reasoning this influence has not been tested yet by comparison with laboratory data on crushed salt specimens with substantially different grain size distribution.

Unfortunately the model on compaction of wet crushed salt has been implemented too late to be tested within the REPOPERM benchmark. The model has been derived independently but is in full accord with other models on diffusional transport creep. So the properties of the model should prove to give similar results as other models do. Due to the hyperbolic stress relation it even includes the possibility to give better results for high stresses. The approach is based on the same geometrical assumptions as in case of dry crushed salt what must not be right. So despite all physical and geometrical reasoning the model still has to be proven by comparison with experimental results.

The relation of permeability as a power of porosity with exponent 5 is based on experimental data from laboratory only. The physical relation may be influenced by the creep rate what has not been investigated sufficiently. Furthermore permeability is assumed to be strongly influenced by humidity. There is good reason to assume that the grain size distribution may essentially change the relation used. So the influence of the physical processes on the geometry of the pores is not understood enough to derive a relation describing the development of permeability. So this phenomenological relation is not supposed to give good results in any case. So in general the evolution of permeability k should be done in the form $dk / d\varepsilon = f\left(\varepsilon, \dot{\varepsilon}, h, ...\right)$. 2-phase-effects have not been taken into account at all. Nevertheless, most of the unknown impacts should in tendency lead

to a more dense material than it is suggested by the simple power relation on porosity. Especially in case of wet conditions compaction might support the total closure of path-ways. In case of 2-phase-flow the permeability will be reduced anyhow.

Dissolution of crushed salt as well as precipitation in a temperature gradient is not taken into account so far.

Literature

/BEH 04/ Bechthold et al.: Backfilling and sealing of underground Repositories for radioactive waste in salt (BAMBUS II Project). Final report. - European Commission, nuclear science and technology, EUR 20621 EN, Luxembourg, 2004.

/HAM 07/ A. Hampel & O. Schulze: The Composite Dilatancy Model: A constitutive model for the mechanical behavior of rock salt. – In: K.-H. Lux, W. Minkley, M. Wallner & H.R. Hardy, Jr. (Hrsg.): Basic and Applied Salt Mechanics; Proc. of the Sixth Conf. on the Mechanical Behavior of Salt (Saltmech 6), Hannover, Mai 2007, S. 99-107, Taylor & Francis (Balkema), London, 2007.

/HEE 89/ Heemann, U., 1989: Transientes Kriechen und Kriechbruch im Steinsalz, Forschungs- und Seminarberichte aus dem Bereich Mechanik der Universität Hannover, Bericht-Nr. F 89/3, Dissertation Nov. 1989

HEI 91/ Hein, H.-J., 1991: "Ein Stoffgesetz zur Beschreibung des thermomechanischen Verhaltens von Salzgranulat", Dissertation, RWTH Aachen

/HUN 81/ Hunsche, U., 1981: Results and Interpretation of Creep Experiments on Rock salt, The Mechanical Behavior of Salt, Proceedings of the First Conference, Trans Tech Publications, 1984, p. 159-167

/HUN 88/ Hunsche, U., 1988: Measurement of Creep in Rock Salt at Small Strain Rates, The Mechanical Behavior of Salt, Proceedings of the Second Conference, Trans Tech Publications, 1988, p. 187-196

/KOR 96/ Korthaus, E., 1996: "Consolidation and deviatoric deformation behaviour of dry crushed salt at temperatures up to 150°C", 4th Conference on the Mechanical Behaviour of Salt, Montreal, 1996, p. 365-377

/STE 85/ Stelte, N., 1985: "Analytische Approximation der Konvergenzrate salzgrusversetzter und unter hydraulischem Druck stehender Hohlräume im

Salzgestein.", Fachband 15 zum Projekt Sicherheitsstudien Entsorgung: Einzeluntersuchungen zur Radionuklidfreisetzung aus einem Modellsalzstock, Abschlußbericht, Berlin, Jan. 1985

/STÜ 95a/ Stührenberg, D.; Zhang, C.-L.: Untersuchungen zum Kompaktionsverhalten von Salzgrus als Versatzmaterial für Endlagerbergwerke im Salz unter besonderer Berücksichtigung der Wechselwirkung zwischen Gebirge und Versatz. BGR-Abschlußbericht zum BMFT-Fv. Förderkennzeichen 02 E 8552 8, Archiv-Nr. 113 259, Hannover, 1995

/STÜ 95b/ Stührenberg, D.; Zhang, C.-L.: Results of Experiments on the Compaction and Permeability Behavior of Crushed Salt. Proc. of the Fifth Intern. Conf. on Radioactive Waste Management and Environmental Remediation, Berlin (ICEM' 95), 1995

Appendix Aa Numerical investigation of the combined hydrostatic / deviatoric stress function

A sphere of radius $R = 1$ is given, modelled in 2D by axis-symmetric finite elements. The radius of a central hollow sphere is defined as $r = 0.04, 0.1, 0.4, 0.8$ in four independent models. The displacements on the surface of this sphere have not been predefined but their radial components were constrained to be proportionally to their distance to the vertical axis of symmetry. In this way an ellipsoidal deformation was guaranteed, facilitating the evaluation of the numerical results. The model has been loaded such that the hydrostatic stress was held constant at 10 MPa (without loss of generality). The deviatoric load is defined by radial and axial stresses and varied such that in the extreme cases either the radial or the axial component was zero. The numerical algorithm was geometrically linear so that the FE model received a stationary state of stress and creep rate. A Norton type salt creep rate was used (see eq. (A1.9)), with a set of parameters for salt that has been published by Hunsche (/HUN 81/), known as BGRa ($A = 0.18\,d^{-1}$, $Q = 54\,kJ\,/\,mol,\ n = 5$ and gas constant R^{gas}=8.3143 $\mathrm{J}/\left(\mathrm{K\ mol}\right)$). The relations

$$\left.\begin{aligned} \dot{\varepsilon}_{\mathrm{vol}} &= \mathrm{A}'\sqrt{\mathrm{a_j\,p^2 + b_j\,q^2}}^{\,4}\sqrt{\mathrm{a_j}}\,\mathrm{p\,c} \\ \dot{\varepsilon}_{\mathrm{dev}} &= \mathrm{A}'\sqrt{\mathrm{a_j\,p^2 + b_j\,q^2}}^{\,4}\sqrt{\mathrm{b_j}}\,\mathrm{q} + \mathrm{A}'\mathrm{q}^5 \end{aligned}\right\}\ \mathrm{j} = 0.04,\ 0.1,\ 0.4,\ 0.8 \qquad (\text{a.1})$$

gave very good results with p and q being the hydrostatic and deviatoric components of the stress field. The parameter $\mathrm{a_j}$ and $\mathrm{b_j}$ showed a different development as a function of void ratio, suggesting a specification for the functions $\mathrm{h_1(e)}$ and $\mathrm{h_2(e)}$ as they are defined in the attempt of Hein (see /HEI 91/) for instance (s. eq. 3.20). For a void ratio $\mathrm{e} \le 1\mathrm{E}-3$ the influence of the hydrostatic and the deviatoric stresses proved to be proportional such that the functions $h_1(e)$ and $h_2(e)$ should differ by a factor of ≈ 1 only. The influence of the deviatoric stress for larger pores increases with the square of the void ratio, while the influence of the hydrostatic stress grows with the third power. A very good approach would be

$$\mathrm{b_j} = 2\,\mathrm{a_j}^{0.64}, \qquad (\text{a.2})$$

leading to a mean deviation of 16% between eq. (a.1) and the numerical results.

Appendix Ab Evaluation of the experimental BGR data on crushed salt

A naive evaluation of the creep curves for crushed salt with technically defined steps in creep rates suggests a stress power of $n \approx 15-20$, which is in contrast to the stress power $n \approx 5$ used for rock salt. Starting point for the new evaluation was the consideration that hardening of the crystals may distinctly influence the power of stress in the case of usual evaluation of data. Frictional forces at oedometer walls have a similar effect, in principle, but numerical analyses by means of a constitutive law defined by eq. (6.1) to (6.6) gave good agreement with experimental data during the increasing load phase, despite the power $n = 5$. Furthermore, the effect of friction at the walls was too small to explain the experimental results. For inserted phases of load relief generally too low stresses have been calculated thus supporting the hardening effect during high load what had not been included in the model so far.

For this purpose, BGR Oedo-49 test data (/STÜ 95b/, $T = 50°C$) have been evaluated such that the stresses for three void ratios ($e = 0.1, 0.2, 0.3$) have been taken from the given curves (see Fig. Ab.1 and Tab. Ab.1) and numerically compared with the theoretical attempt.

The theoretical expectation requires that the compaction rate is given by a Norton-type-attempt for a given compaction state, taking account of a resistive stress σ_R due to hardening.

$$\dot{e} = A_e \left(\sigma - \sigma_R\right)^n \qquad \text{(b.1)}$$

It is assumed for this evaluation that the hardening stress σ_R in the experiment is roughly proportional to the maximum stress achieved so far for the given compaction.

$$\sigma_R \approx z\,\sigma_{\max} \qquad \text{(b.2)}$$

If there is any relief of stress the hardening stress is kept constant for a while and thus the creep rate must decrease much more than it would in the case of no hardening.

Eq. (b.1) involves three parameters (A_e, σ_R, n) so that at least three measured values are needed. The three parameters have been fitted to four values using the least squares method (see Tab. Ab.1). This procedure has been carried out independently for the three void ratios. The resulting values are listed in Tab. Ab.2.

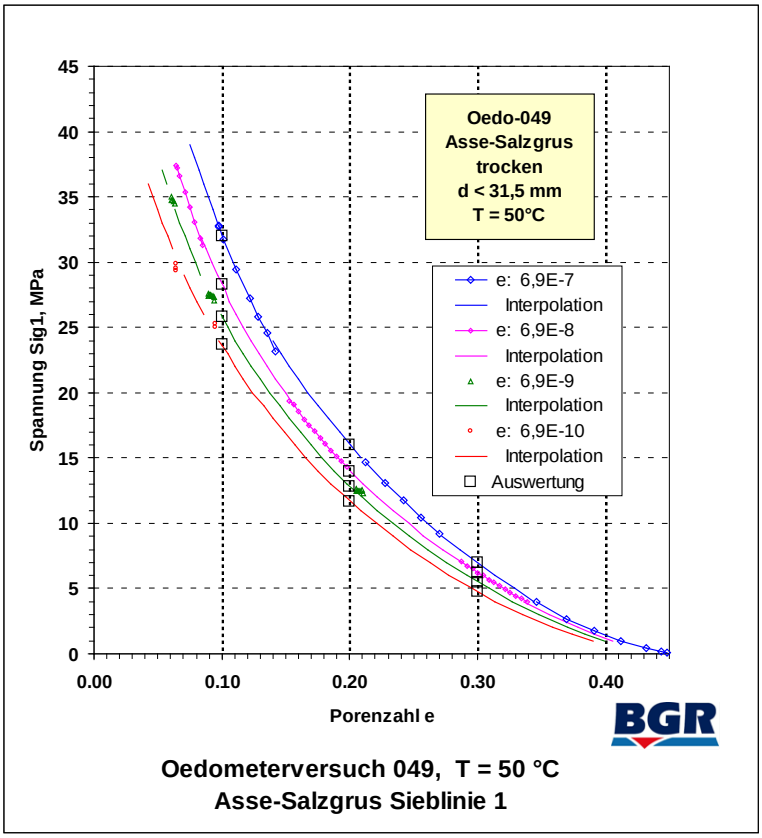

Fig. Ab.1 Plot of chosen values (black squares), listed in Tab. Ab.1. The underlying curves are based on manual interpolation by Stührenberg & Zhang (1995).

Tab. Ab.1: Chosen values from Fig. Ab.1, taken for parameter fit for eq. (b.1).

$\dot{e}\left[s^{-1}\right]$	$\sigma[MPa]$ for $e=0.1$	$\sigma[MPa]$ for $e=0.2$	$\sigma[MPa]$ for $e=0.3$
$6.9E-7$	32	16	7
$6.9E-8$	28	14	6.17
$6.9E-9$	25.8	12.8	5.5
$6.9E-10$	23.7	11.7	4.8

The parameter z describes the relative portion of hardening stress as

$$z = \frac{\sigma_R}{\sigma_{\max}} \qquad \text{(b.3)}$$

where maximal stress is the stress of the upper curve ($\sigma_{\max} = \sigma\left(\dot{e} = 6.9E-7\, s^{-1}\right)$), see Fig. Ab.1 and Tab. Ab.1).

Tab. Ab.2: Parameter for three chosen void ratios requested for eq. (b.1) and (b.2).

Parameter	$e = 0.1$	$e = 0.2$	$e = 0.3$
A_e	4.26E-13	4.88E-10	1.05E-13
σ_R	20.59	11.00	2.69
n	5.87	4.51	10.75
z	0.64	0.69	0.38

For rock salt usually a value of $n_{rock\,salt} \approx 5$ (/HUN 81/) is used and $z_{rock\,salt} \approx 0.6 - 0.7$ (/HUN 88/). The independently found values for $e = 0.1$ and $e = 0.2$ in Tab. Ab.2 are very near to them. A clearly higher stress exponent has been found for a lower hardening stress for a very loose material ($e = 0.3$). But this deviation should not be overvalued considering the imprecise data and further disturbing influences.

Ultimately, these few experiments appear to underline that a description of creep based on hardening is plausible so far and leads to verifiable results already.

Appendix Ac On evolution of hardening stress

Hardening stress can be used for constitutive equations only if there is a model for its evolution with load and time. Here there are two independent models to be deduced. The first serves to describe the physical mechanisms leading to the development of inner hardening stresses in a homogeneously loaded crystal. The second model tries to encompass the very heterogeneous stress distribution within a loaded crystal and the very heterogeneous hardening in a predominantly phenomenological approach.

Ac.1 Physical model based on the development of inner hardening stresses within a crystal

The hardening of a crystal is based on the retarding interaction of the dislocations whose movements directly give rise to deformation. Following the inverse distance dependency of interaction forces between dislocations the hardening stress can be related to the dislocation density ρ. The development of the dislocation density is determined by dislocation multiplication (by means of Frank Read sources) on one hand and dislocation annihilation (mutual erasure of two dislocations of opposite Burgers vector) on the other (see /HEE 89/).

$$\dot{\rho} = \dot{\rho}^{+} - \dot{\rho}^{-} = \kappa^{+} \rho \, \mathrm{v} \, \sigma_{eff} - \kappa^{-} \frac{\rho^2 \, \mathrm{v}}{\sigma_{eff}} \qquad (\text{c.1})$$

The effective stress σ_{eff} is given by the global deviatoric stress minus the hardening stress σ_R.

$$\sigma_{eff} = \left\langle \sigma^{dev} - \sigma_R \right\rangle \qquad (\text{c.2})$$

The angle brackets are Föpplsymbols[2]. The hardening stress is directly related to the dislocation density ρ via some constants (the scalar constant $\alpha \approx 0.15$, the Burgers vector b and the shear modulus G).

$$\sigma_R = \alpha \, b \, G \sqrt{\rho} \qquad (\text{c.3})$$

v (see eq. (c.4)) stands for the medium velocity of the dislocations as a function of the effective stress. κ^{+} and κ^{-} are temperature independent constants. For stationary creep the dislocation density reaches (in consequence of eq. (c.1))

$$\dot{\rho} = 0 \quad \Rightarrow \quad \rho^{stat} = \frac{\kappa^{+}}{\kappa^{-}} \left(\sigma_{eff}^{stat} \right)^2 . \qquad (\text{c.4})$$

---

[2] $f \le 0 \quad \Rightarrow \quad \langle f \rangle = 0$
$f > 0 \quad \Rightarrow \quad \langle f \rangle = f$

So the effective stress in the case of stationary creep is related to the square root of the dislocation density.

$$\sigma_{eff}^{stat} = \sqrt{\frac{\kappa^-}{\kappa^+}\rho^{stat}} \qquad (c.5)$$

The effective stress must be smaller than the macroscopic stress σ^{dev}. So from

$$\sigma_{eff}^{stat} = \sigma^{dev} - \sigma_R^{stat} = (1-z)\sigma^{dev} \qquad (c.6)$$

it can be concluded that the stationary value for the hardening stress is given by

$$\sigma_R^{stat} = z\,\sigma^{dev} \qquad (c.7)$$

where $z < 1$. It can further be deduced via

$$\begin{aligned}\sigma_R^{stat} &= z\,\sigma^{dev} = \alpha\, b\, G\sqrt{\rho^{stat}} = \alpha\, b\, G\sqrt{\frac{\kappa^+}{\kappa^-}}\,\sigma_{eff}^{stat} \\ &= \alpha\, b\, G\sqrt{\frac{\kappa^+}{\kappa^-}}(1-z)\sigma^{dev},\end{aligned} \qquad (c.8)$$

that the constant z is also related to other given constants.

$$\frac{\kappa^+}{\kappa^-} = \left(\frac{z}{\alpha\, b\, G(1-z)}\right)^2 \qquad (c.9)$$

Following the Orowan equation on the relation between the velocity v of the sliding dislocations and the deformation rate

$$\dot{\varepsilon}^{creep} = b\,\rho\,\mathrm{v}, \qquad (c.10)$$

eq. (c.4) can be replaced by

$$\dot{\rho} = \left(\frac{\kappa^+}{b} \sigma_{eff} - \frac{\kappa^-}{b} \frac{\rho}{\sigma_{eff}} \right) \dot{\varepsilon}^{creep} = \frac{\kappa^+}{b} \left(\sigma_{eff} - \frac{\kappa^-}{\kappa^+} \frac{\rho}{\sigma_{eff}} \right) \dot{\varepsilon}^{creep} . \qquad (c.11)$$

To avoid the somewhat "abstract" dislocation densities use can be made of the relationship between hardening stress and dislocation density. Its rate (see eq. (c.3), (c.11) and (c.9)) results in

$$\begin{aligned} \dot{\sigma}_R &= \frac{\alpha b G}{2} \frac{\dot{\rho}}{\sqrt{\rho}} = \frac{\alpha b G}{2} \frac{\kappa^+}{b} \frac{\left(\sigma_{eff} - \frac{\kappa^-}{\kappa^+} \frac{\rho}{\sigma_{eff}} \right) \dot{\varepsilon}^{creep}}{\sqrt{\rho}} \\ &= \frac{\kappa^+ (\alpha b G)^2}{2b} \frac{\left(\sigma_{eff} - \frac{\kappa^-}{\kappa^+ (\alpha b G)^2} \frac{\sigma_R^2}{\sigma_{eff}} \right)}{\sigma_R} \dot{\varepsilon}^{creep} \\ &= \kappa \frac{\left(\sigma_{eff} - \left(\frac{1-z}{z} \right)^2 \frac{\sigma_R^2}{\sigma_{eff}} \right)}{\sigma_R} \dot{\varepsilon}^{creep} \end{aligned} \qquad (c.12)$$

with the constant

$$\kappa = \frac{\kappa^+ (\alpha b G)^2}{2b} . \qquad (c.13)$$

Eq. (c.12) can be transformed to the differential equation

$$\frac{d\sigma_R}{d\varepsilon^{creep}} = \kappa \left(\frac{\sigma_{eff}}{\sigma_R} - \left(\frac{1-z}{z} \right)^2 \frac{\sigma_R}{\sigma_{eff}} \right) . \qquad (c.14)$$

For stationary creep a constant relationship between effective and hardening stress is the result

$$\frac{d\sigma_R}{d\varepsilon^{creep}} = 0 \quad \Rightarrow \quad \left(\frac{\sigma_{eff}}{\sigma_R} \right)^2 = \left(\frac{1-z}{z} \right)^2 . \qquad (c.15)$$

in agreement with eq. (c.6) and (c.7). The prefactor should be in the order of $\kappa \approx 100$. The value of the relative portion of the hardening stress to the macroscopic deviatoric stress has been found experimentally to be $z \approx 0.7$ (/HUN 88/).

Ac.2 Phenomenologically based model on the development of inner hardening stress in the contact zone of a crushed salt grain

In the contact zone of the idealized crushed salt crystal (see Fig. A.1) strongly hardened parts are combined with those parts that have come into the contact zone during the recent process of deformation. A precise capture of this heterogeneous hardening distribution is almost impossible. To get near to this process of hardening the following considerations will be placed at the beginning of this chapter:

– During ongoing compaction of the crushed salt the contact area will permanently broaden and thus reduce the effective local stress.
– This is also true for a constant rate of compaction with increasing global load, because the local strain rate, and thus the effective stress, can steadily decrease with increasing height of the contact zone.
– Highly hardened zones will not deform any more when the stress is reduced below the local hardening stress.
– If the local stress is below the hardening stress the non-hardened zones below will continue to creep. The creep rate is then very slow so that it has been assumed here that under in-situ conditions creep will cease de facto.

The geometrically idealized crystal model will be used once more to model heterogeneous hardening. In the case of edged grain geometry (see Fig. A.1) the height ratios of h'' and h' are always

$$\frac{h''}{h'} = \frac{1}{3}. \qquad \text{(c.16)}$$

The compaction can be taken as roughly proportional to $h'\text{-}h'' = (2/3)h'$. When the contact zone completely covers new portions of the pyramidal structure (see Fig. Ac.1) the width and the height h' have grown by a factor of 1.5.

It can now be assumed that after such a strong deformation, when the deformed volume has tripled, the influence of the former contact zone has almost vanished and the salt newly entered into the contact zone will determine the creep ability.

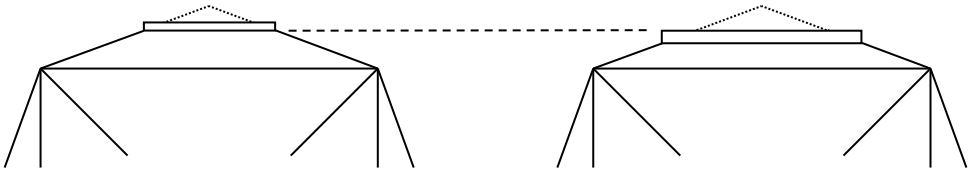

Fig. Ac.1 Illustration of the relative change of geometry for which an accommodation of hardening to the changed stress will have happened.

Because there is no relationship to the absolute size of the contact zone it can be safely assumed that the process is principally the same for any level of deformation irrespective of details of the process. This means that for the accommodation of hardening stress the amount of further deformation will approximately be half of the deformation so far.

So it is assumed here that the accommodation is proportional to the ongoing compaction $d\varepsilon_v$.

$$d\sigma_{RV} = -k\left(\sigma_{RV} - z\,\sigma\right) d\varepsilon_v \qquad \text{(c.17)}$$

The proportionality constant should be roughly given by

$$k \approx \frac{1}{m\,\varepsilon_v} \qquad \text{(c.18)}$$

with a value of $m \approx 0.5$ (or less!) according to the upper reasoning.

Appendix Ad On grain rearrangement

When describing grain rearrangement in a loose, uncompacted, crushed salt one should initially assume the grains as pure elastic bodies with a defined coefficient of friction. If a global load is applied some grains will slip, depending on their relative position but independent of the value of the load. This means that this process will occur for a very small load but stops after a relatively short rearrangement, because rearrangement can only be active as long as the ratio of shear stress to vertical stress is lower than the coefficient of friction. Further slip is not possible even for raising loads.

Under these circumstances compaction by rearrangement would in fact be a negligible process because gravitation already (mostly) will have had such a short effect. Thus further compaction by rearrangement due to slip as a result of an increase of hydrostatic pressure cannot be anticipated. So a relevant rearrangement can only be explained by the action of inelastic deformation.

Rearrangement can be stated if there is a sudden displacement of adjoining grains, probably connected with a certain amount of rotation, leading to a higher coordination number (number of adjoining grains in contact) and a smaller volume per grain.[3] As a result of this definition creep does not incorporate any rearrangement.

Although rearrangement is not associated with creep it is effectively connected with a reduction of the initial void space. Rearrangement can have a volumetric as well as a deviatoric component. But only the volumetric component changes the initial void ratio.

Nevertheless, if shear forces are enhanced in relation to normal forces further relevant compaction by slip and roll movements can be achieved. However, it must be noted that this is not possible without breaking junctions that have been formed by creep deformation. With ongoing deformation this effect should become more and more difficult.

---

[3] The change of the coordination number here only indirectly is taken into account, if ever. It might be related to the parameter γ which influences the relative area U' in a non-linear way and may be attributed to an increase in the number of contacts.

Inelastic effects such as creep and fracture are necessary to achieve grain rearrangement. The effective forces in the contact zone can be attributed to the local stress σ_{local}. It comprises pure pressure as well as shear stress (see definition in eq. (3.4)). Though friction may not allow local slip, rearrangement can happen by fracture or – possibly, to a minor amount – deformation.

Three phenomena can be assumed as reasons for rearrangement:

1. Displacement as a consequence of asymmetrically distributed contacts.

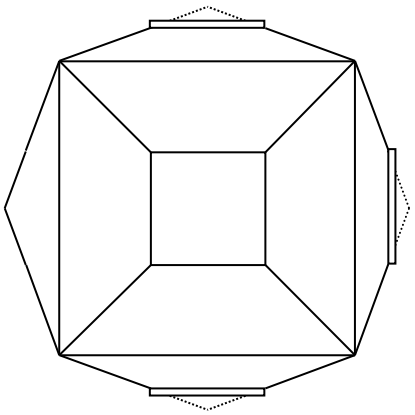

Fig. Ad. 1 Asymmetric deformation can lead to a directed displacement of a grain by pure creep.

Grain displacement by asymmetric creep deformation is assumed to be rather rare. This contribution will not explicitly be taken into account here but is considered as part of usual creep.

2. Displacement due to fracture.

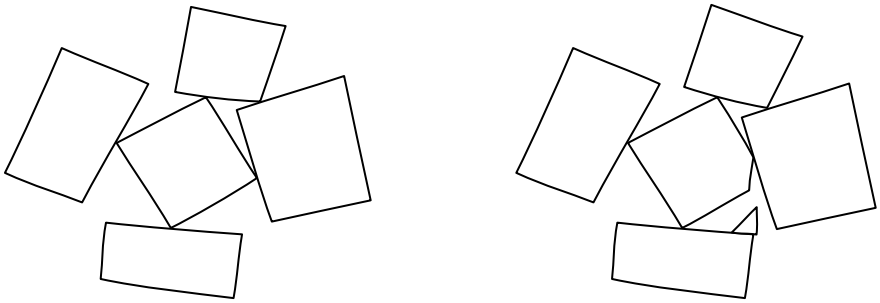

Fig. Ad. 2 Grain displacement due to local fracture.

Fracture is supposed to happen when the local stress exceeds a certain threshold which, from a theoretical point of view, is similar to the behaviour of ideal plasticity. In the context of continuum mechanics plastic deformation or creep usually is defined via potentials (here $G^{\#}(\sigma_{local})$).

$$\dot{\varepsilon}_{ij}^{\#} \square G^{\#}\left(\sigma_{local}\right)\frac{\partial G^{\#}\left(\sigma_{local}\right)}{\partial \sigma_{local,ij}} \qquad (d.1)$$

It is assumed that the process of fracture and the resulting deformation mostly is restricted to the contact zone. The influence of geometry should therefore be of approximately the same nature as in the case of creep (see. eq. (6.1) and (6.2)). Thus a development of rate is given by

$$\dot{\varepsilon}_{ij}^{\#} = B^{\#}\, G^{\#}\left(\sigma_{local}\right)\cot\left(\alpha\right)\sqrt{U}\, e\frac{\frac{1}{k}+e}{1+e}\frac{\partial G^{\#}\left(\sigma_{local}\right)}{\partial \sigma_{local,ij}} \qquad (d.2)$$

with the potential

$$G^{\#}\left(\sigma_{local}\right) = \left\langle \sigma_{local} - \sigma_{\#} \right\rangle . \qquad (d.3)$$

The constant $B^{\#}$ does not show any temperature dependency for creep. The Föppl braces (see eq. (d.3)) ensure that fracture occurs only after reaching fracture stress

$\sigma_{\#}$. So, essentially, the local stresses cannot exceed the fracture stress, controlled by the parameter $\mathrm{B}^{\#}$ which determines how rapidly the stress is decreasing to fracture stress again. $B^{\#} = \infty$ would correspond to a plastic deformation such that the stress is strictly bound to the yield point (or below).

The function $\cot(\alpha)\sqrt{\mathrm{U}}$ is associated with the relative size of the contact zone. The proportionality in e (see eq. (d.2)) attributes to the reduced effect for low porosity. A nonlinear relation on e cannot be excluded. The next term as a function of $1/\mathrm{k}$ and e accounts for the division into compacting and non-compacting grains, depending on grain size distribution.

The linear dependency of the fracture strain rate (eq. (d.2)) on stress (eq. (d.3)) accounts for the expectation that the process can be simplified this way in the relevant stress regime, irrespective of any existing non-linearity. The fracture stress $\sigma^{\#}$ should primarily correspond to the fracture stresses found in short-term laboratory experiments. However, the fact that scientific experience shows that the fracture stress is inversely proportional to the square root of the grain size must be taken into account.[4] The fracture stress can be estimated as

$$\sigma^{\#} = \sigma_o^{\#} \sqrt{\frac{10\,mm}{D_i}} \qquad (\text{d.4})$$

with the additional constant

$$\sigma_o^{\#} \approx 20\,MPa\,. \qquad (\text{d.5})$$

D_i is regarded as an effective diameter of the governing small grains. This effective diameter should also be taken for humidity creep (see below). Eqs. (d.4) with (d.5) would also correspond to typical compact rock salt.

The derivation of the potential to the local stresses is given by

[4] This relationship can also be justified theoretically.

$$\frac{\partial G^{\#}\left(\sigma_{local}\right)}{\partial \sigma_{local,ij}} = \frac{1}{\sigma_{local}}\left(\frac{p}{U'}\frac{\delta_{ij}}{3} + \sqrt{b}\,\frac{q_{ij}}{U'^{\beta}}\right). \qquad (d.6)$$

3. Displacement by roll effects, still connected to break up of existing junctions.

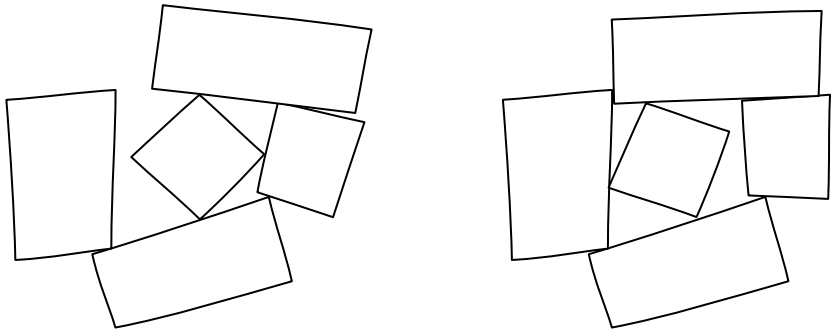

Fig. Ad. 3 Grain rearrangement by rotation, triggered by local shear.

True roll movement does happen and locally may account for a reduction of void space. But in most cases pure roll movement is connected with an increase of the adjacent pores – at least temporarily. In a dense heap of debris there is no space for such movement. But it will occur to a minor degree in conjunction with fracture. If so, its volumetric, as well as deviatoric, effect can be taken as implicitly included in eq. (d.2).

Integration into the crushed salt model

For volumetric and deviatoric deformation the creep and fracture deformation rates are simply to be added.

$$\begin{aligned} \Delta\varepsilon_{vol} &= \frac{\Delta e}{1+e} = \left(\dot{\varepsilon}_{vol}^{creep} + \dot{\varepsilon}_{vol}^{\#}\right)\Delta t \\ \Delta\varepsilon_{dev} &= \left(\dot{\varepsilon}_{dev}^{creep} + \dot{\varepsilon}_{dev}^{\#}\right)\Delta t \end{aligned} \qquad (d.7)$$

But it is crucial for the use of grain rearrangement by fracture that the reduction of volume also reduces the initial volume.

$$\Delta e_o = \dot{\varepsilon}_{vol}^{\#}\left(1+e\right)\Delta t \qquad (d.8)$$

Appendix Ae On the evaluation of the fraction 1/k of small grains

In the case of ideal Fuller distribution it must be assumed that the finer grains always fill the remaining space between the coarser ones down to the lower edge of the curve. If this distribution stops at the diameter of the finest grains its size also is representative for the size of the pores.[5] Furthermore the boundary between those grains that are assumed to deform and those that almost don't should not be too far from the lower limit of the distribution (see Fig. Ae.1). Here a factor of 2 or 3 is assumed to be adequate.

The crushed salt used by Korthaus (/KOR 96/) is most probably characterised by the grain size distribution shown below (Fig. Ae.1, blue line). The measured values (blue squares) differ in diameter by a factor of 2 from one square to the next. The additionally inserted Fuller curve (red line) demonstrates that this reference is of restricted validity.

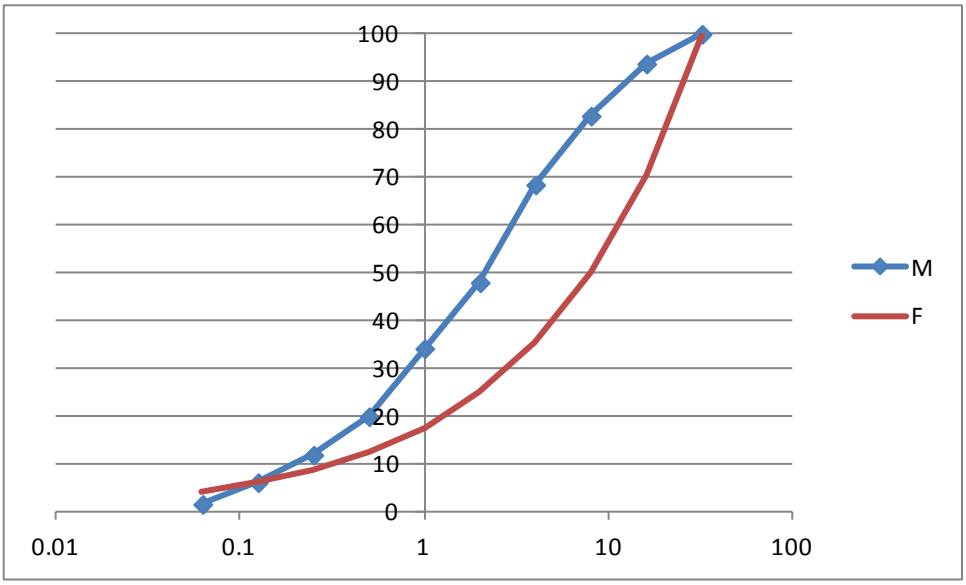

Fig. Ae.1 Korthaus' grain size distribution curve compared to the theoretical Fuller curve (red).

The comparison can be improved by use of a double logarithmic plot (see Fig. Ae.2). As long as the distribution curve is roughly parallel to the theoretical Fuller curve, the space

[5] The pore diameter should be 30% to 100% of the smallest grain diameter.

filling effect of the finer grains is maintained. Fig. Ae.2 shows that the effective limit can be assumed to be approximately at a grain diameter $D \leq 0.2\,mm$. For a factor of 2 related to that diameter a relative proportion of mass of fine grains is found to be 0.17, about equivalent to a value of $k \approx 6$.

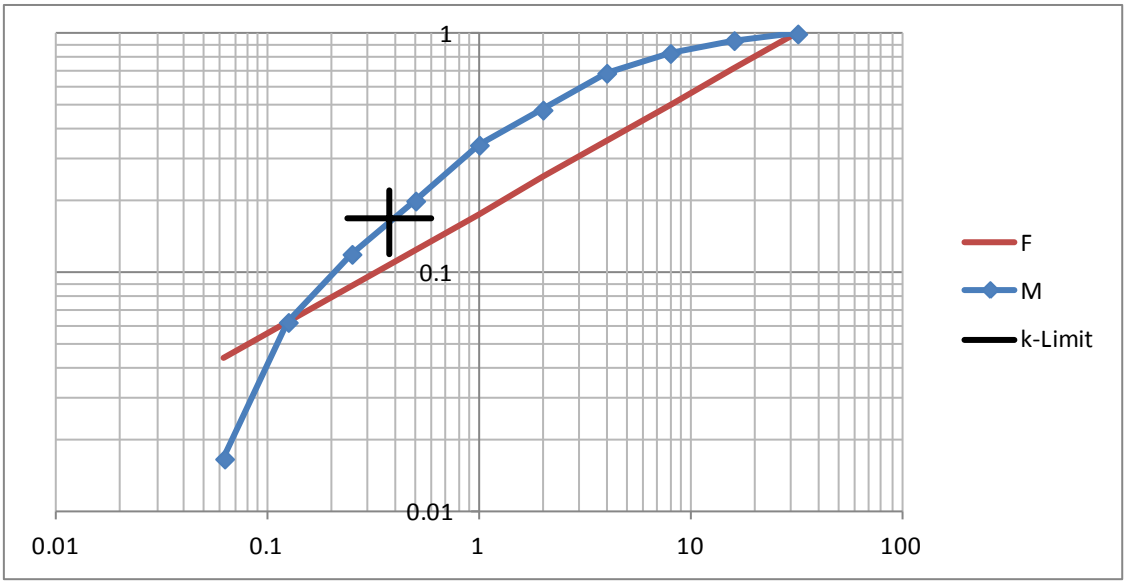

Fig. Ae.2 Comparison of the grading curve in Fig. Ae.1 and the Fuller distribution in a double logarithmic plot. Furthermore, the assumed limit between compacting and non-compacting grains (k-Limit) is marked by a cross.

Appendix Af On determining a parameter set for k=6

Fig. Af.1 shows the parameters of the list in Tab. A.1 as acquired for $k = 1$, $k = 3$ and $k = 24.63$. Furthermore, the values have been expanded by additional parameters for $k = 6$ such that they fit to interpolated quadratic curves. Fig. Af.2 shows that the interpolation also assumes a plausible curvature in the case of a double logarithmic plot. The resulting values are incorporated in Tab. A.1.

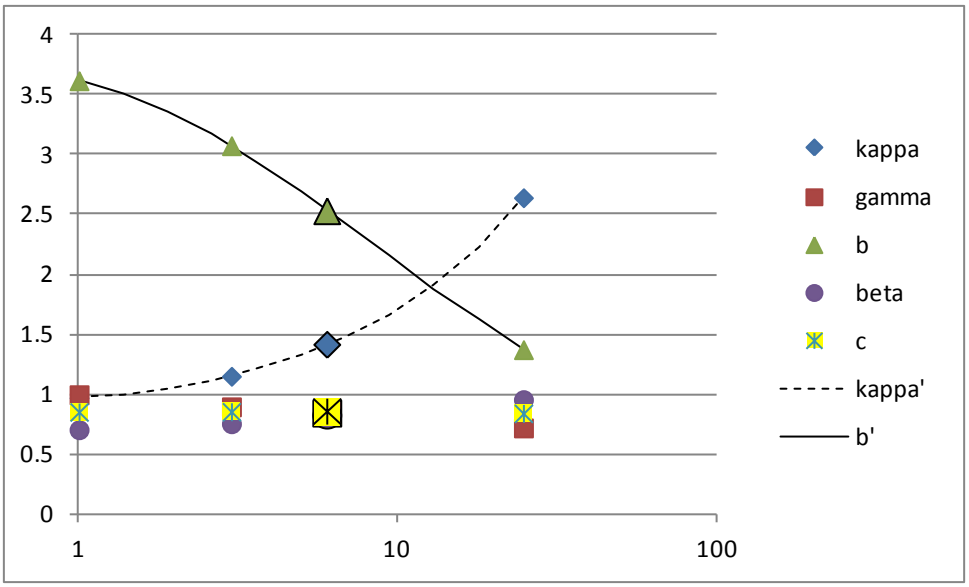

Fig. Af.1 Optimised parameters for $k=1$, $k=3$ and $k=24.63$. For $k=6$ the parameters have been incorporated assuming that the parameters have a smooth curvature as functions of k. The development is effectively linear over $\log(k)$ for the parameters γ, β and c, while non-linear interpolation functions have been used for κ and b. The interpolated values for $k=6$ are highlighted by large symbols.

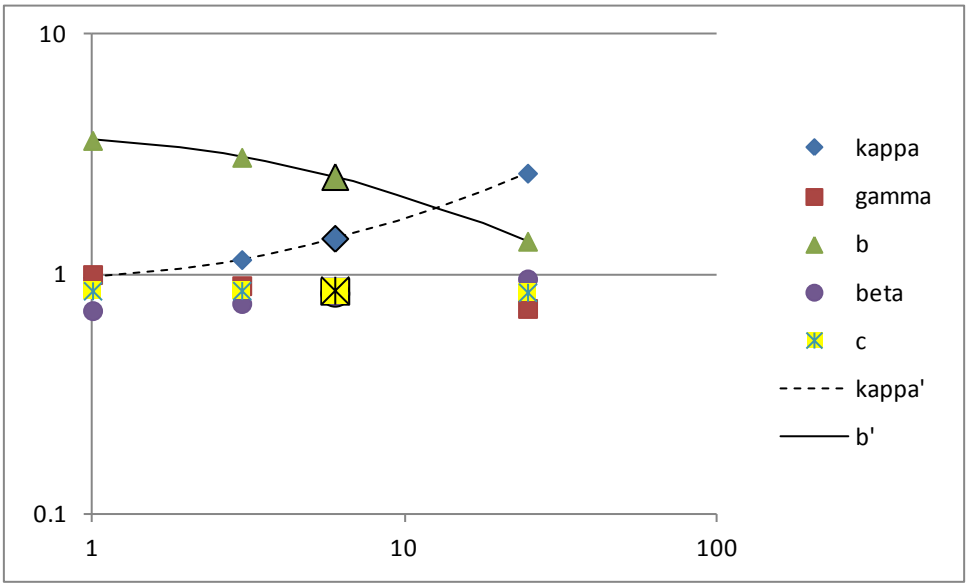

Fig. Af.2 The same plot as in Fig. Af.1, but in double logarithmic form. The quadratic interpolation functions used here also form the basis for the plot in Fig. Af.1.

Appendix Ag Elastic stiffness of crushed salt

The stored elastic energy in a model crystal can be calculated by integration over stresses and volume. It is given by

$$W = \int_V \frac{\sigma^2}{2C} dV = \int_{\Delta h} \frac{\sigma^2}{2C} A\, dh \qquad (g.1)$$

with the elastic stiffness C and the cross sectional area A. The axial force resulting from global stresses is constant within the total body. So the energy W is given by

$$\begin{aligned} F &= \sigma_{global}\, D^2 = \sigma_{global}\, D_i^2 \left(1+\cot(\alpha)\right)^2 \left(\frac{1+k\,e}{1+k\,e_o}\right)^{2/3} = \sigma\, A = const \\ \Rightarrow \quad W &= \int_{\Delta h} \frac{F^2}{2C\,A} dh = \frac{F^2}{2C} \int_{\Delta h} \frac{1}{A} dh = \frac{F^2}{2C} I\,. \end{aligned} \qquad (g.2)$$

The stress within the body is essentially related to the local area of the cross section, also depending on the current degree of compaction. Compaction can be fixed by the value of (see eq. (A1.4) and (A1.5))

$$\mathrm{y} = \frac{\mathrm{s}'}{\mathrm{D_i}} = \frac{2\,\mathrm{h}'}{\mathrm{D_i}\cot(\alpha)} = \frac{3}{2}\frac{1+\cot(\alpha)}{\cot(\alpha)}\left(1-\left(\frac{1+\mathrm{k\,e}}{1+\mathrm{k\,e_o}}\right)^{1/3}\right). \qquad (g.3)$$

There are four different geometric regimes.

In the contact zone the cross section is constant.

$$A = s'^2 = D_i^2\, y^2 \qquad (g.4)$$

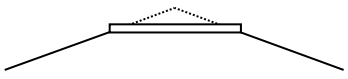

Fig. Ag.1 Lateral view of the contact volume.

The integral is given by the following eq. (g.2) and the relationship $h' = s' \cot(\alpha)/2$ (see eq. (A1.4))

$$I_1 = \int_0^{\frac{1}{3}h'} \frac{1}{A}\, dh = \frac{s' \cot(\alpha)}{6 s'^2} = \frac{\cot(\alpha)}{6 s'} = \frac{\cot(\alpha)}{6 D_i\, y}. \qquad \text{(g.5)}$$

In the pyramidal region the cross section increases quadratically with

$$A = s'^2 \left(\frac{h}{h'}\right)^2 \Bigg|_{h'}^{D_i \cot(\alpha)/2} = D_i^{\,2}\, y^2 \left(\frac{h}{h'}\right)^2 \Bigg|_{h'}^{D_i \cot(\alpha)/2}. \qquad \text{(g.6)}$$

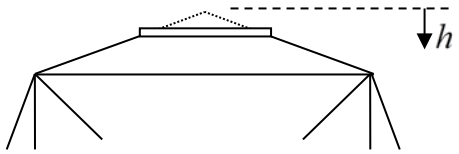

Fig. Ag.2 Lateral view of the pyramidal regime.

The related integral is given by (see also eq. (A1.4))

$$\begin{aligned} I_2 &= \int_{h'}^{D_i \cot(\alpha)/2} \frac{1}{s'^2 \left(\frac{h}{h'}\right)^2} dh = \frac{h'^2}{s'^2} \int_{h'}^{D_i \cot(\alpha)/2} \frac{1}{h^2} dh = -\frac{h'^2}{s'^2} \frac{1}{h} \Bigg|_{h'}^{D_i \cot(\alpha)/2} \\ &= -\frac{h'^2}{s'^2} \left(\frac{2}{D_i \cot(\alpha)} - \frac{1}{h'} \right) = -\frac{\cot(\alpha)^2}{4} \left(\frac{2}{D_i \cot(\alpha)} - \frac{2}{s' \cot(\alpha)} \right) \\ &= -\frac{\cot(\alpha)}{2 D_i} \left(1 - \frac{1}{y} \right). \end{aligned} \qquad \text{(g.7)}$$

In the regime of the core before reaching the next contact zone the cross section comprises the quadratic core and four trapeziums which reach the lateral contact zone at the other end.

$$A = D_i^2 + 4\left(\frac{D_i + D'}{2}\right) z\Big|_0^{(D_i - s')\cot(\alpha)/2} = D_i^2 + 4\left(\frac{D_i + D_i\left(1 - \frac{z}{D_i \cot(\alpha)/2}\right)}{2}\right) z\Big|_0^{(D_i - s')\cot(\alpha)/2} \qquad \text{(g.8)}$$

$$= D_i^2 + 4 D_i \left(1 - \frac{z}{D_i \cot(\alpha)}\right) z\Big|_0^{(D_i - s')\cot(\alpha)/2}$$

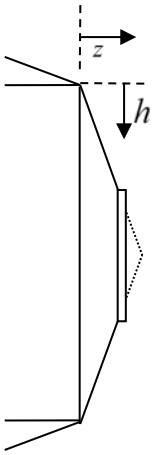

Fig. Ag.3 Lateral view of the outer region of the cross section in the third integration zone.

The length z is coupled to the integration depth h by

$$z = h \cot(\alpha). \qquad \text{(g.9)}$$

The integral is given by

$$I_3 = \frac{1}{D_i} \int_0^{(D_i - s')/2} \frac{1}{D_i + 4\left(1 - 2\frac{h}{D_i}\right) h \cot(\alpha)} dh \qquad \text{(g.10)}$$

$$= \frac{1}{D_i} \int_0^{(1-y)/2} \frac{1}{1 + 4(1 - 2s)\, s \cot(\alpha)} ds$$

and thus results as

$$I_3 = \frac{\operatorname{artanh}\left(\dfrac{\sqrt{\cot(\alpha)}\,(2s-1)}{\sqrt{1+\cot(\alpha)}}\right)}{2D_i\sqrt{\cot(\alpha)}\sqrt{1+\cot(\alpha)}}\Bigg|_0^{(1-y)/2}$$

$$= \frac{1}{2D_i\sqrt{\cot(\alpha)}\sqrt{1+\cot(\alpha)}}\left(\begin{array}{l}\operatorname{artanh}\left(\dfrac{\sqrt{\cot(\alpha)}\;y}{\sqrt{1+\cot(\alpha)}}\right)\\ +\operatorname{artanh}\left(\dfrac{\sqrt{\cot(\alpha)}}{\sqrt{1+\cot(\alpha)}}\right)\end{array}\right). \qquad \text{(g.11)}$$

In the fourth zone the cross section is constant and equal to the highest argument in the integral of I_3 plus four lateral cross sections in the contact zones.

$$A = D_i^2 + 4D_i\left(1-\frac{z}{D_i\cot(\alpha)}\right)z\Big|_{z=(D_i-s')\cot(\alpha)/2} + 4\frac{h'}{3}s' \qquad \text{(g.12)}$$

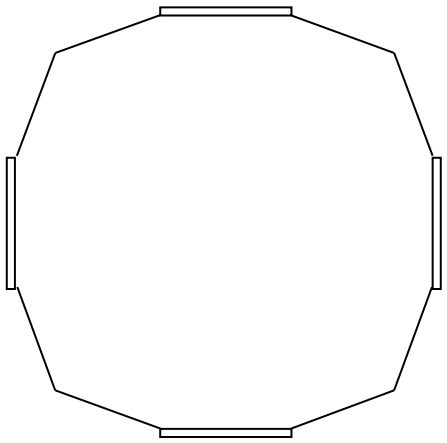

Fig. Ag.4 Vertical view of the cross section in the fourth integration regime.

The inner term in eq. (g.12) can be calculated as

$$
\begin{aligned}
&4 D_i \left(1-\frac{z}{D_i \cot(\alpha)}\right) z \Big|_{z=(D_i-s')\cot(\alpha)/2} \\
&= 2 D_i \left(1-\frac{(D_i-s')\cot(\alpha)/2}{D_i \cot(\alpha)}\right)(D_i-s')\cot(\alpha) \\
&= 2 D_i^2 \left(1-\frac{1-y}{2}\right)(1-y)\cot(\alpha) \\
&= 2 D_i^2 \cot(\alpha)\left(1-y-\frac{1-2y+y^2}{2}\right) = D_i^2 \cot(\alpha)\left(1-y^2\right).
\end{aligned}
\qquad \text{(g.13)}
$$

The right term in eq. (g.12) can be written as

$$
4\frac{h'}{3}s' = \frac{2}{3}s'^2 \cot(\alpha) = D_i^2 \cot(\alpha)\frac{2y^2}{3}. \qquad \text{(g.14)}
$$

So eq. (g.12) is given by

$$
A = D_i^2\left(1+\cot(\alpha)\left(1-y^2+\frac{2y^2}{3}\right)\right) = D_i^2\left(1+\cot(\alpha)\left(1-\frac{y^2}{3}\right)\right). \qquad \text{(g.15)}
$$

Because of the constant cross section and the height s' the fourth integral simply is given by

$$
I_4 = \frac{s'}{D_i^2\left(1+\cot(\alpha)\left(1-\frac{y^2}{3}\right)\right)} = \frac{y}{D_i\left(1+\cot(\alpha)\left(1-\frac{y^2}{3}\right)\right)}. \qquad \text{(g.16)}
$$

The first three regimes have to be taken twice due to reasons of symmetry so that the total integral results in

$$D_i\, I = \frac{2\cot(\alpha)}{3y} - \cot(\alpha)\left(1-\frac{1}{y}\right) + \frac{y}{1+\cot(\alpha)\left(1-\frac{y^2}{3}\right)}$$
$$+\frac{1}{2\sqrt{\cot(\alpha)}\sqrt{2+\cot(\alpha)}}\left(\begin{array}{l}\operatorname{artanh}\left(\dfrac{\sqrt{\cot(\alpha)}\,\left(2(1-y)\cot(\alpha)-1\right)}{\sqrt{2+\cot(\alpha)}}\right)\\ +\operatorname{artanh}\left(\dfrac{\sqrt{\cot(\alpha)}}{\sqrt{2+\cot(\alpha)}}\right)\end{array}\right). \qquad \text{(g.17)}$$

The mean specific energy in the total body must be taken to calculate the total stiffness, that is the energy within the model volume (see eq. (g.12) and (g.17)) of an individual (small) grain as well as the energy of the remaining larger grains. Then it is given by:

$$W_{tot} = \frac{\sigma_{global}^2}{2C'} V_{tot} = \frac{\sigma_{global}^2}{2C} V_{k-1} + \frac{F^2}{2C} I\,. \qquad \text{(g.18)}$$

V_{k-1} is the volume of the large grains, the force F is given by eq. (g.12). So C' is the stiffness of all grains. The total volume is given by

$$V_{tot} = V_{k-1} + V_1\,. \qquad \text{(g.19)}$$

The volume V_1 of the crushed salt grain is defined by (see also eq. (A1.1))

$$\mathrm{V_1} = \mathrm{D_o}^3 \frac{1+\mathrm{k\,e}}{1+\mathrm{k\,e_o}} = \mathrm{D_i}^3 \left(1+\cot(\alpha)\right)^3 \frac{1+\mathrm{k\,e}}{1+\mathrm{k\,e_o}}\,. \qquad \text{(g.20)}$$

Its pure bulk volume $\mathrm{V_S}$ is given by eq. (A1.2). V_{k-1} is given by

$$V_{k-1} = (k-1)V_S\,. \qquad \text{(g.21)}$$

Inserting into eq. (g.18) gives

$$W_{tot} = \frac{\sigma_{global}^2}{2C'}\left((k-1) D_i^3 \left(1+\cot(\alpha)\right) + D_i^3 \left(1+\cot(\alpha)\right)^3 \frac{1+k\,e}{1+k\,e_o} \right)$$

$$= \frac{\sigma_{global}^2}{2C}(k-1) D_i^3 \left(1+\cot(\alpha)\right) + \frac{\left(\sigma_{global}\, D_i^2 \left(1+\cot(\alpha)\right)^2 \left(\frac{1+e}{1+e_o} \right)^{2/3} \right)^2}{2C} I . \qquad \text{(g.22)}$$

Reducing by $\sigma_{global}^2 \; D_i^3 \left(1+\cot(\alpha)\right)/2$ delivers

$$\frac{1}{C'}\left((k-1) + \left(1+\cot(\alpha)\right)^2 \frac{1+k\,e}{1+k\,e_o} \right)$$

$$= \frac{1}{C}\left((k-1) + \left(1+\cot(\alpha)\right)^3 \left(\frac{1+k\,e}{1+k\,e_o} \right)^{4/3} D_i\, I \right) \qquad \text{(g.23)}$$

and so

$$\frac{C'}{C} = \frac{(k-1) + \left(1+\cot(\alpha)\right)^2 \frac{1+k\,e}{1+k\,e_o}}{(k-1) + \left(1+\cot(\alpha)\right)^3 \left(\frac{1+k\,e}{1+k\,e_o} \right)^{4/3} D_i\, I} . \qquad \text{(g.24)}$$

The expression $D_i\, I$ must be replaced by eq. (g.17). The relative stiffness as a function of void ratio for different values of k can be seen in Fig. Ag.5.

The development of relative stiffness for $k = 1$ should, in theory, correspond to the stiffness of a single size distribution. For $k = 3$ (the initially favoured variant) a mostly linear run with void ratio results while the curve for $k = 6$ better corresponds to Hein's curve. Best agreement with Hein's curve would be given for $k = 9$.

Theoretically, the same type of integral ($\int 1/A\,dh$) is needed for the evaluation of thermal conductivity as it appears in eq. (g.12) ff. Regardless of the artificial geometry adopted here, the relative shape should be the same in principle for stiffness and thermal conduc-

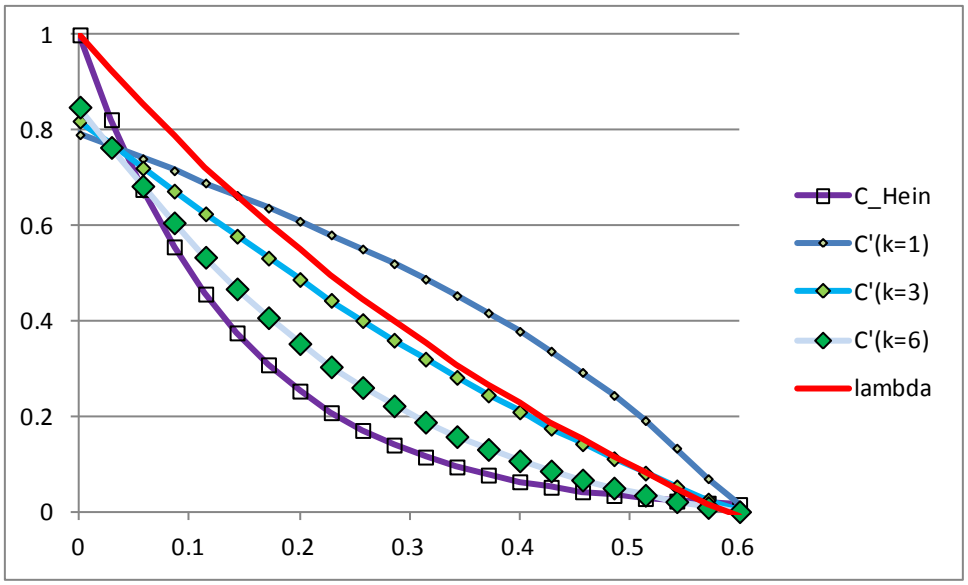

Fig. Ag.5 Plot of the relative stiffness for three different values of the parameter k compared to the Hein's experimentally determined curves as well as compared to the experimentally found relative thermal conductivity of crushed salt.

tivity[6]. So it has been inserted in Fig. Ag.5 for comparison. But it must not be forgotten that eq. (g.24) used here predicts an influence of the grain size distribution in any case, so that a clear conclusion cannot be drawn from the comparison with experimental data as long as the correct value of k is not known.

It must be taken into account that for $y = 1$ (when the contact area is as broad as the lateral faces of the core ($s' = D_i$)) the limits of the geometric model are reached in the treatment used here. This can be seen for very small void spaces only, but causes an obvious deviation from the value 1 for total compaction. However, that does not generally discard the validity of the theoretical results.

The theoretical model can also be used for other initial porosities. In Fig. Ag.6 the initial void ratio has been reduced to 0.3 instead of 0.6. The Hein curves and the thermal conductivity parameters have been changed such that they fit the reduced range of void ratio. The Hein equation is described by an exponential dependency on void number η.

[6] The data have been taken from experimental laboratory data /BAM 04/.

$$\frac{C'}{C} = \exp\left(-c_k \frac{\eta\left(1-\eta_o\right)}{1-\eta} \right) \qquad \text{(g.25)}$$

Following Hein the parameter c_k is

$$10.95 = \frac{0.6567}{0.06} \le c_k \le \frac{0.6567}{0.04} = 16.42\,. \qquad \text{(g.26)}$$

In Fig. Ag.5 the smallest value (10.95) has been used. In Fig. Ag.6 the upper value has been taken with $c_k = 16.42$.

The relative conductivity is described by

$$\frac{\lambda}{\lambda_o} = 1 - 2.7\,\eta\,. \qquad \text{(g.27)}$$

In Fig. Ag.6 a parameter of 4.3 has been used instead of 2.7.

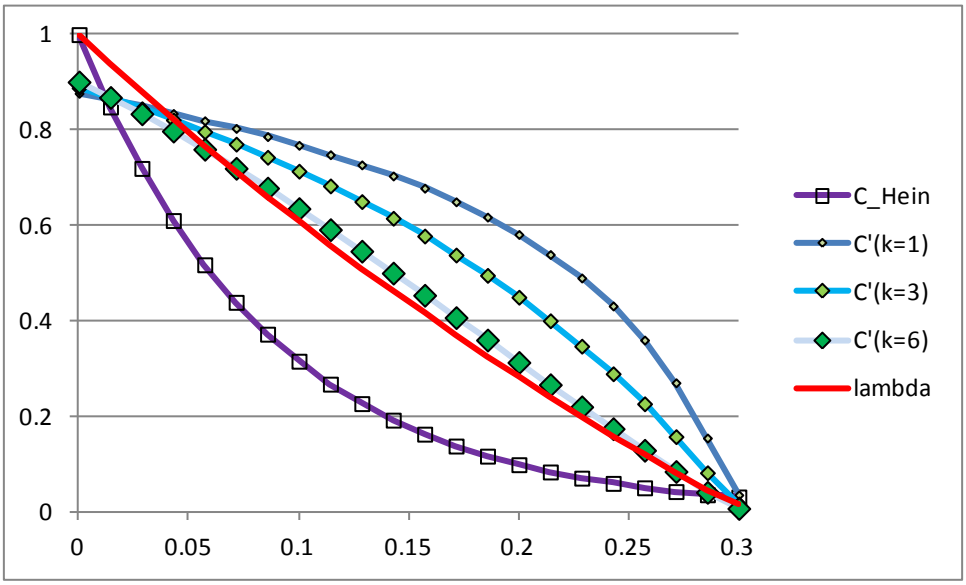

Fig. Ag.6 The same relations as in Fig. Ag.5 but with reduced initial void ratio.

It must be noted that the parameter k has a clear physical meaning, but its value is not yet established and has to be determined for any type of crushed salt. However, knowing this value the stiffness can be calculated for any given initial void ratio.

The initial porosity of loose crushed salt can be reduced by shaking. However, it must be assumed that a broad range of grain sizes with a high value of k is associated to a low initial porosity. So generally a linear characteristic is anticipated for reasons of simplicity if nothing better is known.

Appendix Ah On stress integration for humidity creep

Integration of the differential equation (9.11) over the radius of the contact area gives

$$\int_0^r grad\left(\sigma_n\right) dr = \sigma_n(r) - \sigma_n(0) = \frac{T}{\kappa'}\int_0^r \operatorname{arsinh}\left(\frac{r\,\dot{h}}{2\,b\,D}\exp\left(\frac{Q}{k\,T}\right)\right) dr$$

$$= \frac{T}{\kappa'}\int_0^r \operatorname{arsinh}\left(z\,r\right) dr = \frac{T}{z\,\kappa'}\int_0^{z\,r} \operatorname{arsinh}\left(x\right) dx = \frac{T}{z\,\kappa'}\left(x\operatorname{arsinh}\left(x\right) - \sqrt{x^2+1}\right)\Big|_0^{z\,r} \qquad \text{(h.1)}$$

$$= \frac{T}{z\,\kappa'}\left(\left(z\,r\operatorname{arsinh}\left(z\,r\right) - \sqrt{\left(z\,r\right)^2+1}\right)+1\right)$$

with

$$x = z\,r \qquad \text{(h.2)}$$

and

$$z = \frac{\dot{h}}{2\,b\,D}\exp\left(\frac{Q}{k\,T}\right). \qquad \text{(h.3)}$$

If the contact area is initially subject to a homogeneous pressure distribution, there will be a stress reduction at the outer boundary by means of pressure solution and diffusion of ions to the stress free zone outside. This stress relief will increasingly spread to the inner parts of the contact area. The pressure cannot fall beyond zero. So a stationary state will be characterised by zero pressure at the edge and the radial stress distribution derived above. This means (see eq. (h.1))

$$\sigma_n(R) = \sigma_n(0) + \frac{T}{z\,\kappa'}\left(\left(z\,R\,\mathrm{arsinh}\left(z\,R\right) - \sqrt{\left(z\,R\right)^2+1}\right)+1\right) = 0\,. \qquad \text{(h.4)}$$

Eq. (h.4) offers the possibility to calculate the maximum stress $\sigma_n(0)$.

$$\sigma_n(0) = -\frac{T}{z\,\kappa'}\left(\left(z\,R\,\mathrm{arsinh}\left(z\,R\right) - \sqrt{\left(z\,R\right)^2+1}\right)+1\right) \qquad \text{(h.5)}$$

The total pressure distribution must be in accordance with the mean stress $\bar{\sigma}_n$. It can be calculated using

$$\begin{aligned}\bar{\sigma}_n\,\pi\,R^2 &= \int_0^R 2\,\pi\,r\,\sigma_n(r)\,dr \\ &= \sigma_n(0)\,\pi\,R^2 + \int_0^R 2\,\pi\,r\,\frac{T}{z\,\kappa'}\left(\left(z\,r\,\mathrm{arsinh}\left(z\,r\right) - \sqrt{\left(z\,r\right)^2+1}\right)+1\right)dr\,.\end{aligned} \qquad \text{(h.6)}$$

The equation can be simplified by substituting $x = z\,r$.

$$\begin{aligned}&\int_0^R 2\,\pi\,r\,\frac{T}{z\,\kappa'}\left(z\,r\,\mathrm{arsinh}\left(z\,r\right) - \sqrt{\left(z\,r\right)^2+1}+1\right)dr \\ &= \frac{2\,\pi\,T}{z^3\,\kappa'}\int_0^{z\,R} x\left(x\,\mathrm{arsinh}\left(x\right) - \sqrt{x^2+1}+1\right)dx\end{aligned} \qquad \text{(h.7)}$$

The first part of the integral gives

$$\begin{aligned}\int_0^{z\,R} x^2\,\mathrm{arsinh}\left(x\right)dx &= x^2\left(x\,\mathrm{arsinh}\left(x\right) - \sqrt{x^2+1}\right)\Big|_0^{z\,R} - 2\int_0^{z\,R} x\left(x\,\mathrm{arsinh}\left(x\right) - \sqrt{x^2+1}\right)dx \\ &= x^2\left(x\,\mathrm{arsinh}\left(x\right) - \sqrt{x^2+1}\right)\Big|_0^{z\,R} - 2\int_0^{z\,R} x^2\,\mathrm{arsinh}\left(x\right)dx + 2\int_0^{z\,R} x\sqrt{x^2+1}\,dx.\end{aligned} \qquad \text{(h.8)}$$

The integral to be solved again appears on the right, so that the solution can be found as

$$\int_0^{z\,R} x^2\,\mathrm{arsinh}\left(x\right)dx = \frac{1}{3}\left(x^2\left(x\,\mathrm{arsinh}\left(x\right) - \sqrt{x^2+1}\right)\Big|_0^{z\,R} + 2\int_0^{z\,R} x\sqrt{x^2+1}\,dx\right). \qquad \text{(h.9)}$$

The integral over the square root function

$$\int_0^{zR} x\sqrt{x^2+1}\,dx = \frac{x^2+1}{3}\sqrt{x^2+1}\Big|_0^{zr} \qquad \text{(h.10)}$$

must be inserted in eq. (h.9). It is also found in eq. (h.7).

$$\begin{aligned}
&\int_0^{zR} x\left(x\,\mathrm{arsinh}(x)-\sqrt{x^2+1}+1\right)dx \\
&=\frac{1}{3}\left(x^2\left(x\,\mathrm{arsinh}(x)-\sqrt{x^2+1}\right)\Big|_0^{zR}+2\frac{x^2+1}{3}\sqrt{x^2+1}\Big|_0^{zR}\right)-\frac{x^2+1}{3}\sqrt{x^2+1}\Big|_0^{zR}+\int_0^{zR}x\,dx \\
&=\frac{1}{3}\left(x^2\left(x\,\mathrm{arsinh}(x)-\sqrt{x^2+1}\right)\Big|_0^{zR}-\frac{x^2+1}{3}\sqrt{x^2+1}\Big|_0^{zR}\right)+\frac{x^2}{2}\Big|_0^{zR} \\
&=\frac{1}{3}\left((zR)^3\,\mathrm{arsinh}(zR)-\frac{4(zR)^2+1}{3}\sqrt{(zR)^2+1}\right)+\frac{(zR)^2}{2}+\frac{1}{9}
\end{aligned} \qquad \text{(h.11)}$$

Taking account of eqs. (h.6), (h.5), (h.7) and (h.11), the stress distribution is given by

$$\begin{aligned}
\bar{\sigma}_n\,\pi R^2 &= -\frac{T\,\pi R^2}{z\,\kappa'}\left(\left(zR\,\mathrm{arsinh}(zR)-\sqrt{(zR)^2+1}\right)+1\right) \\
&+\frac{2\pi T}{3z^3\kappa'}\left((zR)^3\,\mathrm{arsinh}(zR)-\frac{4(zR)^2+1}{3}\sqrt{(zR)^2+1}+3\frac{(zR)^2}{2}+\frac{1}{3}\right).
\end{aligned} \qquad \text{(h.12)}$$

Building a help function Y the equation can be simplified

$$Y = \bar{\sigma}_n \pi R^2 \frac{3\kappa'}{T \pi R^3} = \frac{\bar{\sigma}_n 3\kappa'}{T R} = -3\left(\left(\operatorname{arsinh}(X) - \frac{\sqrt{X^2+1}}{X}\right) + \frac{1}{X}\right)$$

$$+2\left(\operatorname{arsinh}(X) - \frac{4X^2+1}{3X^3}\sqrt{X^2+1} + 3\frac{X^2}{2X^3} + \frac{1}{3X^3}\right)$$

$$= -\operatorname{arsinh}(X) + \frac{1}{3X^3}\left(9\left(X^2\sqrt{X^2+1} - X^2\right) - 2\left(4X^2+1\right)\sqrt{X^2+1} + 9X^2 + 2\right) \quad (\text{h.13})$$

$$= -\operatorname{arsinh}(X) + \frac{1}{3X^3}\left(X^2\sqrt{X^2+1} - 2\sqrt{X^2+1} + 2\right)$$

$$= -\operatorname{arsinh}(X) + \frac{1}{3X^3}\left((X^2-2)\sqrt{X^2+1} + 2\right)$$

where

$$X = z R. \quad (\text{h.14})$$

It can easily be shown (see Fig. Ah.1) that over a very large range ($0 \le X \le 100000$) the following approximation can be performed with an error of less than 2%.

$$Y = -\operatorname{arsinh}(X) + \frac{1}{3X^3}\left((X^2-2)\sqrt{X^2+1} + 2\right) \approx -\operatorname{arsinh}(0.75X) \quad (\text{h.15})$$

If the mean pressure, the temperature and the current radius are known, the function of dissolution z can directly be calculated by means of eq. (h.15).

$$z R = X \cong -\frac{4}{3}\sinh(Y) \quad \Rightarrow \quad z \cong -\frac{4}{3R}\sinh(Y) \quad (\text{h.16})$$

Taking into account eq. (h.13) and the definition of Y in eq. (h.13) a relationship between the rate of height $\dot{h}$ and the mean stress $\bar{\sigma}_n$ can be determined

$$\frac{\dot{h}}{2bD}\exp\left(\frac{Q}{kT}\right) \cong -\frac{4\sinh\left(\frac{\bar{\sigma}_n 3\kappa'}{T R}\right)}{3R} \quad (\text{h.17})$$

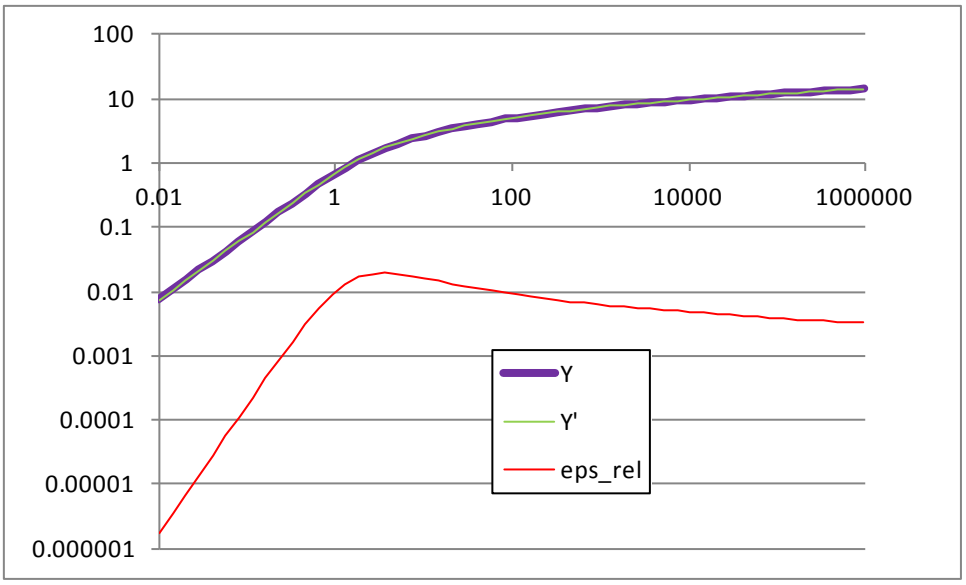

Fig. Ah.1 Plot of the function $|Y|$ over normalised radius and its approximation function $|Y'| = \operatorname{arsinh}(0.75\,X)$, with a maximum relative error of less than 2% (red line).

and thus finally

$$\dot{h} \cong -2.7\,\frac{b}{R}\,D\exp\left(\frac{-Q}{k\,T}\right)\sinh\left(\frac{\bar{\sigma}_n\,3\kappa'}{T\,R}\right). \qquad \text{(h.18)}$$